ENGINEERING OF
BIOMATERIALS
INŻYNIERIA BIOMATERIAŁÓW
JOURNAL OF POLISH SOCIETY FOR BIOMATERIALS AND FACULTY OF MATERIALS SCIENCE AND CERAMICS / AGH UNIVERSITY
CZASOPISMO POLSKIEGO STOWARZYSZENIA BIOMATERIAŁÓW I WYDZIAŁU INŻYNIERII MATERIAŁOWEJ I CERAMIKI / AGH

Number 170
Numer 170
Volume XXVI
Rocznik XXVI

Year 2023
(Issue 3)
Rok 2023
(Zeszyt 3)

ISSN 1429-7248

PUBLISHER:
WYDAWCA:

Polish Society for Biomaterials in Krakow
Polskie Stowarzyszenie Biomateriałów w Krakowie

EDITORIAL COMMITTEE:
KOMITET REDAKCYJNY:

Editor-in-Chief
Redaktor naczelny
Elżbieta Pamuła

Editor
Redaktor
Patrycja Domalik-Pyzik

Secretary of editorial
Sekretarz redakcji
Design
Projekt
Katarzyna Trała

ADDRESS OF EDITORIAL OFFICE:
ADRES REDAKCJI:

AGH University of Krakow
30/A3, Mickiewicz Av.
30-059 Krakow, Poland
Akademia Górniczo-Hutnicza
al. Mickiewicza 30/A-3
30-059 Kraków

Issue: 250 copies
Nakład: 250 egz.

Scientific Publishing House AKAPIT
Wydawnictwo Naukowe AKAPIT
e-mail: wn@akapit.krakow.pl

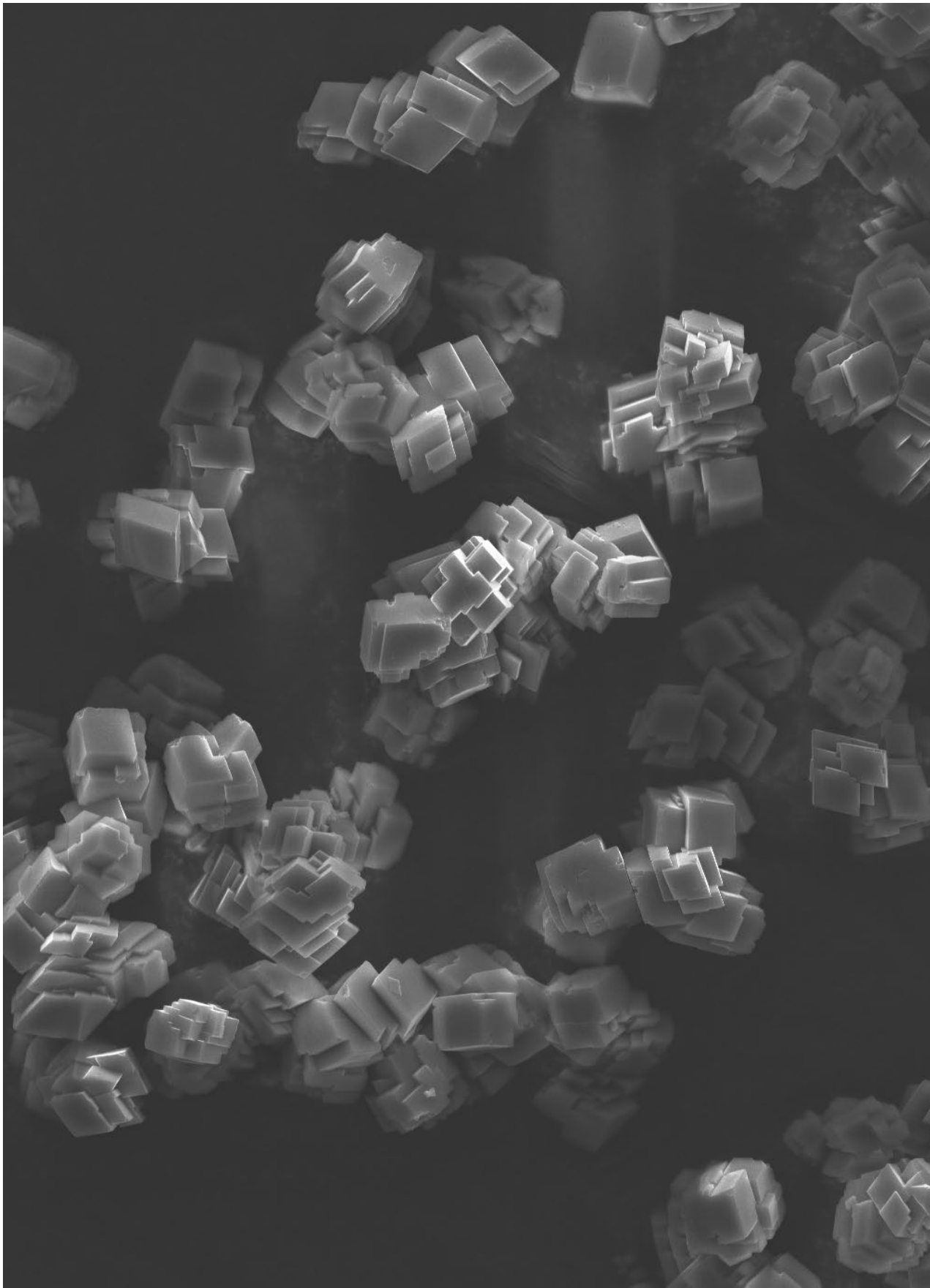

ENGINEERING OF BIOMATERIALS

EDITORIAL BOARD
KOMITET REDAKCYJNY

INTERNATIONAL EDITORIAL BOARD
MIĘDZYNARODOWY KOMITET REDAKCYJNY

ENGINEERING OF BIOMATERIALS

Wskazówki dla autorów

1. Prace do opublikowania w kwartalniku „Engineering of Biomaterials / Inżynieria Biomateriałów" przyjmowane będą wyłącznie w języku angielskim.
2. Wszystkie nadsyłane artykuły są recenzowane.
3. Materiały do druku prosimy przysyłać za pomocą systemu online (www.biomaterials.pl).
4. Struktura artykułu:
• TYTUŁ • Autorzy i instytucje • Streszczenie (200-250 słów) • Słowa kluczowe (4-6) • Wprowadzenie • Materiały i metody • Wyniki i dyskusja • Wnioski • Podziękowania • Piśmiennictwo
5. Autorzy przesyłają pełną wersję artykułu, łącznie z ilustracjami, tabelami, podpisami i literaturą w jednym pliku. Artykuł w tej formie przesyłany jest do recenzentów. Dodatkowo autorzy proszeni są o przesłanie materiałów ilustracyjnych (rysunki, schematy, fotografie, wykresy) w oddzielnych plikach (format np. .jpg, .gif., .tiff, .bmp). Rozdzielczość rysunków min. 300 dpi. Wszystkie rysunki i wykresy powinny być czarno-białe lub w odcieniach szarości i ponumerowane cyframi arabskimi. W tekście należy umieścić odnośniki do rysunków i tabel.
6. Na końcu artykułu należy podać wykaz piśmiennictwa w kolejności cytowania w tekście i kolejno ponumerowany.
7. Redakcja zastrzega sobie prawo wprowadzenia do opracowań autorskich zmian terminologicznych, poprawek redakcyjnych, stylistycznych, w celu dostosowania artykułu do norm przyjętych w naszym czasopiśmie. Zmiany i uzupełnienia merytoryczne będą dokonywane w uzgodnieniu z autorem.
8. Opinia lub uwagi recenzentów będą przekazywane Autorowi do ustosunkowania się. Nie dostarczenie poprawionego artykułu w terminie oznacza rezygnację Autora z publikacji pracy w naszym czasopiśmie.
9. Za publikację artykułów redakcja nie płaci honorarium autorskiego.
10. Adres redakcji:

Czasopismo
„Engineering of Biomaterials / Inżynieria Biomateriałów"
Akademia Górniczo-Hutnicza im. St. Staszica
Wydział Inżynierii Materiałowej i Ceramiki
al. Mickiewicza 30/A-3, 30-059 Kraków
tel. (48) 12 617 44 48, 12 617 25 61
e-mail: epamula@agh.edu.pl, kabe@agh.edu.pl

Szczegółowe informacje dotyczące przygotowania manuskryptu oraz procedury recenzowania dostępne są na stronie internetowej czasopisma:
www.biomaterials.pl

Instructions for authors

1. Papers for publication in quarterly journal „Engineering of Biomaterials / Inżynieria Biomateriałów" should be written in English.
2. All articles are reviewed.
3. Manuscripts should be submitted to editorial office through online submission system (www.biomaterials.pl).
4. A manuscript should be organized in the following order:
• TITLE • Authors and affiliations • Abstract (200-250 words) • Keywords (4-6) • Introduction • Materials and Methods • Results and Discussion • Conclusions • Acknowledgements • References
5. All illustrations, figures, tables, graphs etc. preferably in black and white or grey scale should be additionally sent as separate electronic files (format .jpg, .gif., .tiff, .bmp). High-resolution figures are required for publication, at least 300 dpi. All figures must be numbered in the order in which they appear in the paper and captioned below. They should be referenced in the text. The captions of all figures should be submitted on a separate sheet.
6. References should be listed at the end of the article. Number the references consecutively in the order in which they are first mentioned in the text.
7. The Editors reserve the right to improve manuscripts on grammar and style and to modify the manuscripts to fit in with the style of the journal. If extensive alterations are required, the manuscript will be returned to the authors for revision.
8. Opinion or notes of reviewers will be transferred to the author. If the corrected article will not be supplied on time, it means that the author has resigned from publication of work in our journal.
9. Editorial does not pay author honorarium for publication of article.
10. Address of editorial office:

Journal
„Engineering of Biomaterials / Inżynieria Biomateriałów"
AGH University of Krakow
Faculty of Materials Science and Ceramics
30/A-3, Mickiewicz Av., 30-059 Krakow, Poland
tel. (48) 12) 617 44 48, 12 617 25 61
e-mail: epamula@agh.edu.pl, kabe@agh.edu.pl

Detailed information concerning manuscript preparation and review process are available at the journal's website:
www.biomaterials.pl

STUDIA PODYPLOMOWE
Biomateriały – Materiały dla Medycyny
2023/2024

Organizator: Akademia Górniczo-Hutnicza im. Stanisława Staszica w Krakowie Wydział Inżynierii Materiałowej i Ceramiki Katedra Biomateriałów i Kompozytów **Kierownik:** prof. dr hab. inż. Elżbieta Pamuła **Sekretarz:** dr inż. Katarzyna Reczyńska-Kolman	**Adres:** 30-059 Kraków, Al. Mickiewicza 30 Pawilon A3, p. 208 lub p. 210 tel. 12 617 44 48, 12 617 23 38 email: epamula@agh.edu.pl; kmr@agh.edu.pl https://www.podyplomowe.agh.edu.pl/studia-podyplomowe-kursy-doksztalcajace-i-szkolenia/biomaterialy-materialy-dla-medycyny/
Charakterystyka: Tematyka prezentowana w trakcie zajęć obejmuje przegląd wszystkich grup materiałów dla zastosowań medycznych: metalicznych, ceramicznych, polimerowych, węglowych i kompozytowych. Słuchacze zapoznają się z metodami projektowania i wytwarzania biomateriałów a następnie możliwościami analizy ich właściwości mechanicznych, właściwości fizykochemicznych (laboratoria z metod badań: elektronowa mikroskopia skaningowa, mikroskopia sił atomowych, spektroskopia w podczerwieni, badania energii powierzchniowej i zwilżalności) i właściwości biologicznych (badania: *in vitro* i *in vivo*). Omawiane są regulacje prawne i aspekty etyczne związane z badaniami na zwierzętach i badaniami klinicznymi (norma EU ISO 10993). Słuchacze zapoznają się z najnowszymi osiągnięciami w zakresie nowoczesnych nośników leków, medycyny regeneracyjnej i inżynierii tkankowej.	
Sylwetka absolwenta: Studia adresowane są do absolwentów uczelni technicznych (inżynieria materiałowa, technologia chemiczna), przyrodniczych (chemia, biologia, biotechnologia) a także medycznych, stomatologicznych, farmaceutycznych i weterynaryjnych, pragnących zdobyć, poszerzyć i ugruntować wiedzę z zakresu inżynierii biomateriałów i nowoczesnych materiałów dla medycyny. Słuchacze zdobywają i/lub pogłębiają wiedzę z zakresu inżynierii biomateriałów. Po zakończeniu studiów wykazują się znajomością budowy, właściwości i sposobu otrzymywania materiałów przeznaczonych dla medycyny. Potrafią analizować wyniki badań i przekładać je na zachowanie się biomateriału w warunkach żywego organizmu. Ponadto słuchacze wprowadzani są w zagadnienia dotyczące wymagań normowych, etycznych i prawnych niezbędnych do wprowadzenia nowego materiału na rynek. Ukończenie studiów pozwala na nabycie umiejętności przygotowywania wniosków do Komisji Etycznych i doboru metod badawczych w zakresie analizy biozgodności materiałów.	
Zasady naboru: Termin zgłoszeń: od 20.09.2023 do 20.10.2023 (liczba miejsc ograniczona - decyduje kolejność zgłoszeń) Wymagane dokumenty: dyplom ukończenia szkoły wyższej Osoby przyjmujące zgłoszenia: prof. dr hab. inż. Elżbieta Pamuła (pawilon A3, p. 208, tel. 12 617 44 48, e-mail: epamula@agh.edu.pl) dr inż. Katarzyna Reczyńska-Kolman (pawilon A3, p. 210, tel. 12 617 23 38, e-mail: kmr@agh.edu.pl)	
Czas trwania: 2 semestry (od XI 2023 r. do VI 2024 r.) 8 zjazdów (soboty-niedziele) 1 raz w miesiącu przewidywana liczba godzin: 160	**Opłaty:** 3 000 zł (za dwa semestry)

33rd Biomaterials in Medicine and Veterinary Medicine

Annual Conference

10 – 13 October 2024 Rytro, Poland

SAVE THE DATE

10-13

OCTOBER

2024

www.biomat.agh.edu.pl

REGISTER

AND

SUBMIT

AN ABSTRACT

SPIS TREŚCI
CONTENTS

Wersja papierowa czasopisma „Engineering of Biomaterials / Inżynieria Biomateriałów" jest jego wersją pierwotną
Printed version of „Engineering of Biomaterials / Inżynieria Biomateriałów" is a primary version of the journal

THERMAL AND PHYSICOCHEMICAL PROPERTIES OF SILICONE-BASED COMPOSITES REINFORCED WITH SILANIZED MAGNETIC POWDER

Anna Powojska*, Joanna Niewęgłowska, Joanna Mystkowska

Department of Biomaterials and Medical Devices,
Institute of Biomedical Engineering,
Faculty of Mechanical Engineering,
Bialystok University of Technology,
Wiejska 45C, 15 351 Bialystok, Poland
*e-mail: anna.powojska@pb.edu.pl

Abstract

Silicone-based materials are of great interest in medicine and cosmetic applications because of their biocompatibility and elasticity. Recently, there has been a significant focus on the development of functional materials that integrate multiple desirable characteristics. Elastic composites reinforced with magnetic filler are active in a magnetic field. These materials can be an interesting alternative to the currently used materials, after appropriate modification of the NdFeB powder. From the point of view of the use of materials in biomedical engineering, they require a lot of research and analysis to determine whether they are useful and will not cause potentially negative effects on a living organism. The aim of the work was to verify the influence of the powder silanization method on the thermal and physicochemical properties of silicone-based composites reinforced with NdFeB powder. The appropriate selection of the silanization parameters used in the process allows control of the properties of the composite. The powder surface silanization execution affects the physicochemical and thermal stability of the prepared composites. It has been established that, depending on the method of silanization, the composite properties were changed. The obtained experimental results may lead to further research on the functionalization of elastic composites reinforced with magnetic powder.

***Keywords**: silanization, elastic magnetic composite, thermal properties, physicochemical properties*

Introduction

Silicone materials are commonly used in a variety of medical and cosmetic applications. Nowadays, they are applied mainly outside the body, as materials for contact lenses or artificial skin. However, they can also be used in other medical applications, such as drug delivery systems, cochlear implants, and cardiology. Their biocompatibility with the human body was confirmed in many experimental tests [1,2].

[Engineering of Biomaterials 170 (2023) 2-8]

doi:10.34821/eng.biomat.170.2023.2-8

Submitted: 2023-08-28, Accepted: 2023-09-26, Published: 2023-09-30

High elasticity and ability of silicone-based magnetic composites to move and act in a magnetic field make them of interest in many branches of medicine and biomedical engineering. In the group of elastic polymers, one of the most commonly used is polydimethylsiloxane (PDMS). This polymer is most often combined with highly magnetic particles, e.g. NdFeB [3]. However, the use of NdFeB-based composites in medicine is not widespread, especially due to the risk of adverse reactions in contact with the human body [4-6]. In our previous work [7] the chemical stability of PDMS-based composites was assessed. It was stated that the incubation affects the samples and liquids, changing their physicochemical properties. It is because the organic matrix is lipophilic and the NdFeB powder is hydrophilic, so the compatibility between these two phases is not enough. It can be improved, for example, through modification of the powder surface using the silanization process. The surface modification of the magnetic powder using a biofunctional silane coupling agent enhances the adhesion between the NdFeB particles and the polymer matrix. It was also stated [8] that the addition of a silane coupling agent has almost no effect on the magnetic properties of bonded magnets based on silanized NdFeB magnetic powder and organic binder.

During the silanization process, the magnetic powder surface is coated with alkoxysilane molecules of organofunctional character, as it was described elsewhere [9,10]. This method is commonly used in materials science applications, especially during composites and smart materials preparation. Silanization is successfully implemented, for example, in carbon nanotubes to change the behavior of their surface [11]. This method is also used for the modification of silica wafers to activate their surfaces [12].

Silanization is carried out using chemical compounds called silanes. An example of such a chemical is APTES, which is 3-aminopropyltriethoxysilane with an amino group attached to the silicone chain. APTES is used to modify iron oxide nanoparticles, nanosilica particles, or carbon nanotubes [11,13,14].

The aim of the work was the evaluation of the influence of magnetic powder silanization parameters on the properties of silicone composites, especially their interaction with incubation fluids. This is particularly relevant in biomedical applications.

Materials and Methods

In this study, elastic silicone-based composites reinforced with magnetic powder subjected to the silanization process were examined. The organic matrix used for composite synthesis was Ecoflex 00-30 (Smooth-On, USA). The material belongs to the Ecoflex polymers group, which includes commercially available silicones with varying Shore-A hardness [15]. The silicone used in this study is characterized by a hardness of 30 Shore A. This polymer is prepared from two components, supplied as A and B liquid parts. To obtain the correct mixture, the ingredients must be mixed in a 1A:1B ratio.

Magnetic NdFeB powder (MQFP-14-12, Magnequench, Singapore) with a particle size of d50 = 25 μm (at least 50% of the powder particles have a particle size of 25 μm or less) was the object of the silanization. The chemical composition of the NdFeB powder is presented in TABLE 1.

TABLE 1. Composition of MQFP-14-12 micro-powder.

Element	Fe	Nd	B	Nb
Concentration [%w/w]	71.7	26.0	1.0	1.9

Firstly, micropowder was subjected to the silanization process. The silane used in the experiment was (3-Aminopropyl) triethoxysilane (APTES, Sigma Aldrich, USA). Twelve different combinations of silanization parameters (TABLE 2) were used to modify the surface of the magnetic powder: a) various silane concentrations, b) silanization time, and c) the type of solution used to dilute the silane. Each silanized micropowder was mixed with liquid silicone in a mass ratio of 7:3. Finally, twelve composites (symbols B-M, TABLE 2) based on silanized micropowders were obtained. The sample marked with the symbol C was prepared in two steps. At first, the powder was phosphorated using 10% orthophosphoric acid to activate the surface, and in the second step, silanization was carried out in the ethanol/water mixture. Composites with non-silanized metal powder (symbol A) and pure PDMS (symbol 0) were used as references.

TABLE 2. Silanization parameters used in experiments.

Designation	Silanization parameters		
	Silane concentration [% w/v]	Time, t [h]	Solution type
0	-	-	-
A	-	-	-
B	4.75	>24	ethanol 95%v/v/ water 5%v/v
C	4.75	>24	ethanol 95%v/v/ water 5%v/v (preceded by soaking the powder in 10% orthophosphoric acid)
D	2	4	water
E	2.5	1	toluene
F	2.5	2	
G	2.5	4	
H	5	1	
I	5	2	
J	5	4	
K	7.5	1	
L	7.5	2	
M	7.5	4	

The prepared samples were left for the curing process, and then the samples were cut into smaller pieces, weighed, and divided into two groups: incubated and non-incubated. The samples from the first group were immersed in a 0.9% w/v sodium chloride aqueous solution (NaCl, Sigma Aldrich, USA) prepared with ultrapure Milli-Q water (Merck Millipore, Germany). The second set of samples was stored in a dry place at room temperature.

According to the ISO 10933-13 standard [16], the mass ratio of the composite to the incubation fluid was 1g:10ml. Conditioning studies were carried out in an incubator with an internal temperature range of 37 ± 0.5°C. The materials were incubated for 28 days. After this time, the samples were taken out and dried at room temperature (21 ± 1°C) and 60% humidity for 24 hours.

Thermal properties

The thermal properties of the obtained composites were evaluated using a Q500 thermogravimetric analyzer (TA Instruments, USA). Thermogravimetric tests (TGA) were performed according to the ISO 11358-1:2022 standard [17]. Each measurement was carried out in a nitrogen atmosphere, with a temperature range of 25 to 950°C and a heating rate of 10°C/min. Samples with an average weight of 5 mg were used for testing. Measurements were performed three times for each sample.

Physicochemical properties

The physicochemical properties of the obtained composites were also determined in this study. A water contact angle was measured and analyzed using a contact angle goniometer (Ossila, UK). The contact angle was defined between the surface and the water droplet [18]. The test included applying a 5 µl deionized water droplet on the surface and the drop image on the surface was recorded for 5 s. The obtained images were analyzed with the included software, where a tangent method was used to calculate the water contact angle [19]. Measurements were performed five times for each sample.

The density of the composite was determined using the hydrostatic method. A balance with special equipment and software (Mettler Toledo, USA) enables the calculation of density from the mass of the sample in two density-known environments. The mass of the sample in air and then in water is registered by the device. The density calculation using Archimedes' principle is conducted automatically by the balance. Measurements were made five times for each sample.

Fluid absorption was measured using an analytical balance (Mettler Toledo, USA) with readability up to 0.01 mg. The mass of each sample was recorded before incubation and 24 hours after removal from the containers and drying at room temperature (temperature of 21 ± 1°C and humidity of 60%). The percent change in mass was calculated from equation (1):

$$W(\%) = \frac{w_w - w_d}{w_d} \cdot 100\% \quad (1)$$

where:
w_w - mass of the sample after incubation [g];
w_d - mass of the dry sample before incubation [g].

The measurements were performed five times for each sample.

Surface roughness

The Confocal Laser Scanning Microscopy (CLSM) technique was used for microscopic observations and roughness measurements of the surface. The microscope used in this study was LEXT OLS 4000 (Olympus, Japan). Two linear roughness parameters: Ra - the arithmetic mean value of deviation from the mean surface profile line and Rz - the highest roughness height according to the 10 highest measured profiles, were evaluated [20]. From the 3D images, it was possible to measure three surface roughness parameters: Sa - the arithmetic mean height value of the absolute deviations of the surface, Sq - the mean squared deviation of the surface from the reference surface (standard deviation of the height of surface irregularities), Sp - height parameter of the highest peak of the surface [21]. The parameters were determined using microscope software. It enables an automatic calculation of the roughness on a specific line or surface. Linear measurements were made horizontally. Area measurements were made over an area of 300x300 pixels. Measurements were performed five times for each sample.

Statistical analysis

The results of the measurements are presented as mean values with standard deviations. The r-Pearson correlation test was performed to measure the linear correlation between tested parameters.

Results and Discussion

In this work, the influence of magnetic powder silanization on the thermal and physicochemical properties of silicone-based composites for biomedical applications was determined. The results of thermogravimetric analysis (FIG. 1) allow for the determination of the decomposition temperature at 1 wt% and 5 wt% for all samples before and after incubation.

For most tested samples, 1 wt% weight loss (FIG. 1a) was observed in a temperature range of 200-250°C, both for incubated and non-incubated ones. The only exception was for samples after the silanization and phosphorylation process, marked as C, where the temperature of thermal degradation was ~112°C before and ~105°C after incubation. It was even 100°C lower than for most samples. It may be concluded that the decomposition temperature of the material is lower after silanization combined with phosphorylation. The highest temperatures, although almost at the same level for non-incubated and incubated samples, were observed for the composite with non-silanized micropowder (accordingly ~255°C and ~254°C). However, for the rest of the tested samples, incubation changed the thermal stability of the composites, as the temperatures for 1 wt% weight loss for samples after incubation were lower (from 6°C to 45°C) compared to the non-incubated samples.

In the temperature range of 300-350°C, a 5 wt% weight loss (FIG. 1b) was observed for most of the examined samples, both before and after the incubation process. A similar observation, as for 1 wt% weight loss was for sample C, based on powder after silanization and phosphorylation, where the temperature reached the lowest value (~263°C before and ~252°C after incubation). Generally, the temperature of thermal decomposition after incubation was lower by about 2-28°C compared to the samples before incubation.

In the FIG. 2a the results of density before and after 28 days incubation are presented. The lowest density is obtained for pure silicone (1.04 g/cm^3 before and 1.03 g/cm^3 after incubation). The highest density was measured for the composite (A) with non-silanized NdFeB micropowder (1.70 g/cm^3 before and 1.79 g/cm^3 after incubation) and for sample (I) based on micropowder silanized for 2 h with 5% w/v APTES solution (1.81 g/cm^3 before incubation). The samples prepared with the micropowders silanized in toluene have a density in the range of 1.47-1.62 g/cm^3. The methods using ethanol and water as APTES solvents (B-D) resulted in the lowest density values. In general, it was observed that after incubation of the samples, the density of the tested composites decreased. This may be due to the dissolution of the composite components in sodium chloride solution, which was also observed in the literature [22].

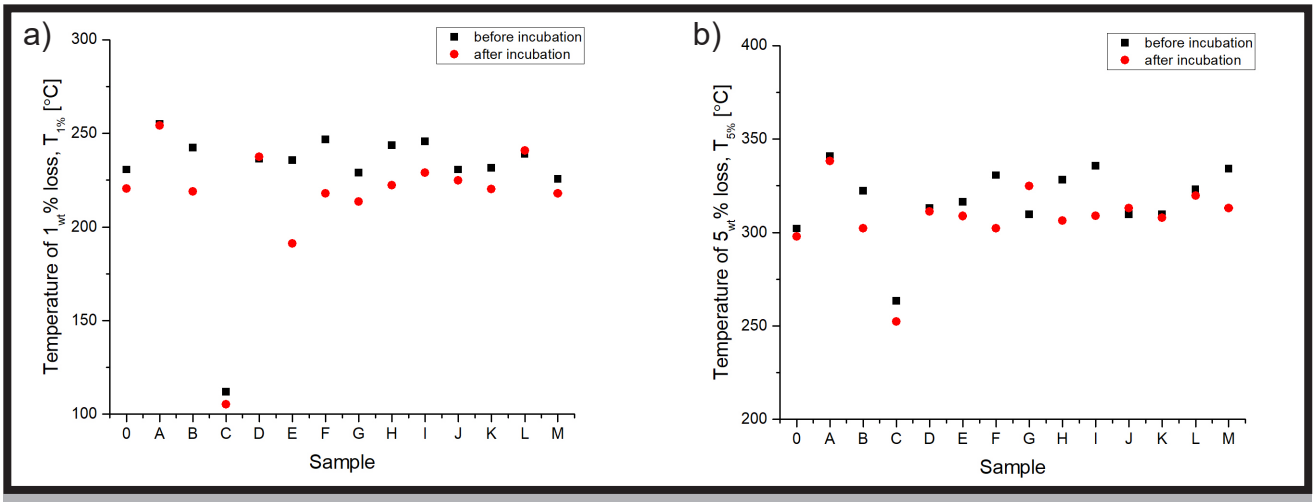

FIG. 1. Results of TGA analysis, (a) 1 wt% and (b) 5 wt% weight loss for samples before and after materials incubation.

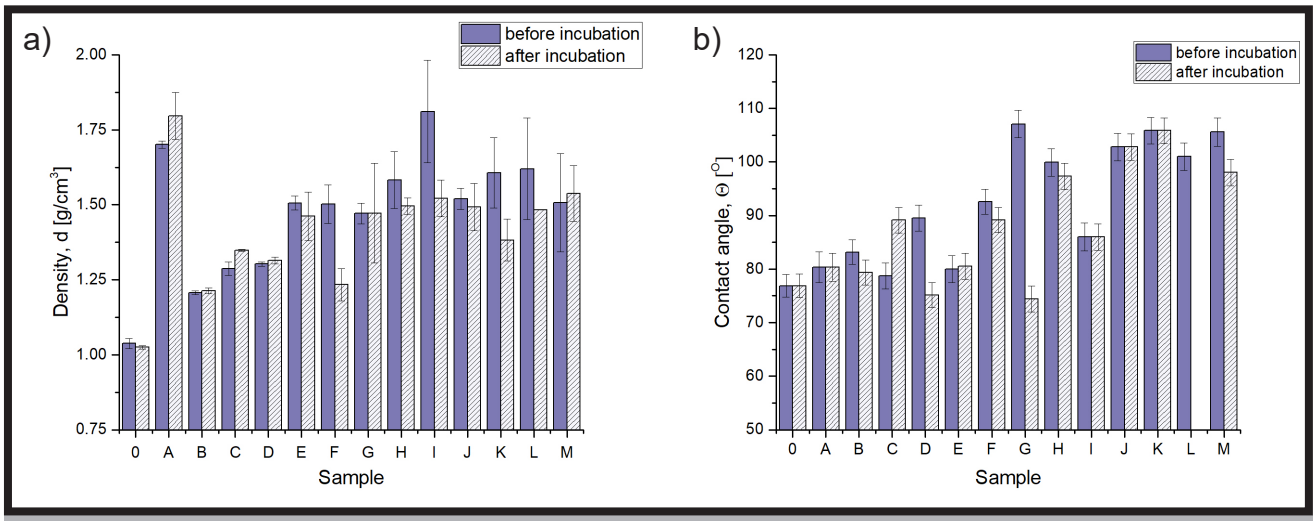

FIG. 2. (a) Density and (b) the water contact angle of the examined composites before and after incubation.

The water contact angle values on the composites before and after incubation are presented in FIG. 2b. The pure silicone (0) tends to be hydrophilic, showing a contact angle value below 90° (Θ = 77° before and Θ = 72° after the incubation process). The addition of micropowder increases the value of the contact angle. For samples, where the powder was silanized with a 5 % w/v (H, J) or 7.5 % w/v (K-M) APTES solution, the water contact angle was higher than 100°. After incubation, this parameter was more stable for samples prepared using ethanol and water as solvents for APTES, where the change in the water contact angle was in the range of 3-12°. A much greater decrease was observed for samples with powder silanized in toluene (E-M). The difference in the contact angle of the sample before and after incubation was, for example, ~32° for sample G and ~46° for sample K. It can be seen that in several cases the material retained its hydrophobic character after incubation. It is reported in the literature that the presence of silane in the composite increases the wettability of a given surface [23,24].

The results of the water absorption of incubated samples are presented in FIG. 3. The lowest percentage of mass change is measured for pure silicone (-0.003%). It was noticed that the longer the silanization time of the micropowders, the higher the water absorption. For sample (E), after 1 h of silanization with 2.5 % w/v of APTES (E), a mass increase of 0.033% was observed. For sample (G) silanized with the same amount of APTES, but for 4 h, a mass increase of 0.050% was observed. A relatively high absorption value was observed for samples with micropowder silanized in ethanol and phosphorated (~0.081%). All examined composites showed a very low level of water absorption after 28 days of the incubation process.

In FIG. 4 results of Ra and Rz linear roughness of composite surface before and after silanization are presented. The highest Ra value was obtained for sample (A) with non-silanized powder (0.25 μm before and 0.17 μm after incubation) and the composite silanized and phosphorated (C) in one process (0.19 μm before incubation). For the rest of the samples, the Ra value did not exceed 0.1 μm. However, it was observed that the silanization method influenced the surface roughness of the incubated samples. Composites prepared with powder silanized in ethanol/water solutions (samples B-D) showed lower Ra value after incubation. For the samples with micropowder silanized in toluene (samples E-M) Ra roughness was lower after incubation.

Similar observations were noted for Rz roughness. The highest Rz value was observed for sample (A) with non-silanized powder (1.58 μm before and 0.85 μm after incubation) and sample (C) silanized and phosphorated in one process (1.25 μm before incubation). For most samples Rz roughness did not exceed 0.3 μm. Similarly to the Ra roughness, for the same composites, incubation causes an increase in the Rz roughness of the materials, which is also observed in other studies in the literature [25,26]. However, for the composite with non-silanized reinforcement (A) and composites with a silanized filler using ethanol or water as solvents (samples B-D), a decrease in surface roughness Rz was observed after incubation [27].

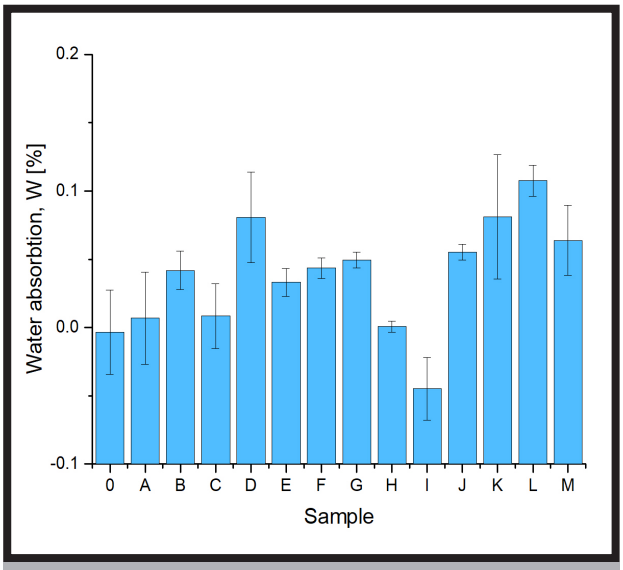

FIG. 3. Water absorption of examined composites.

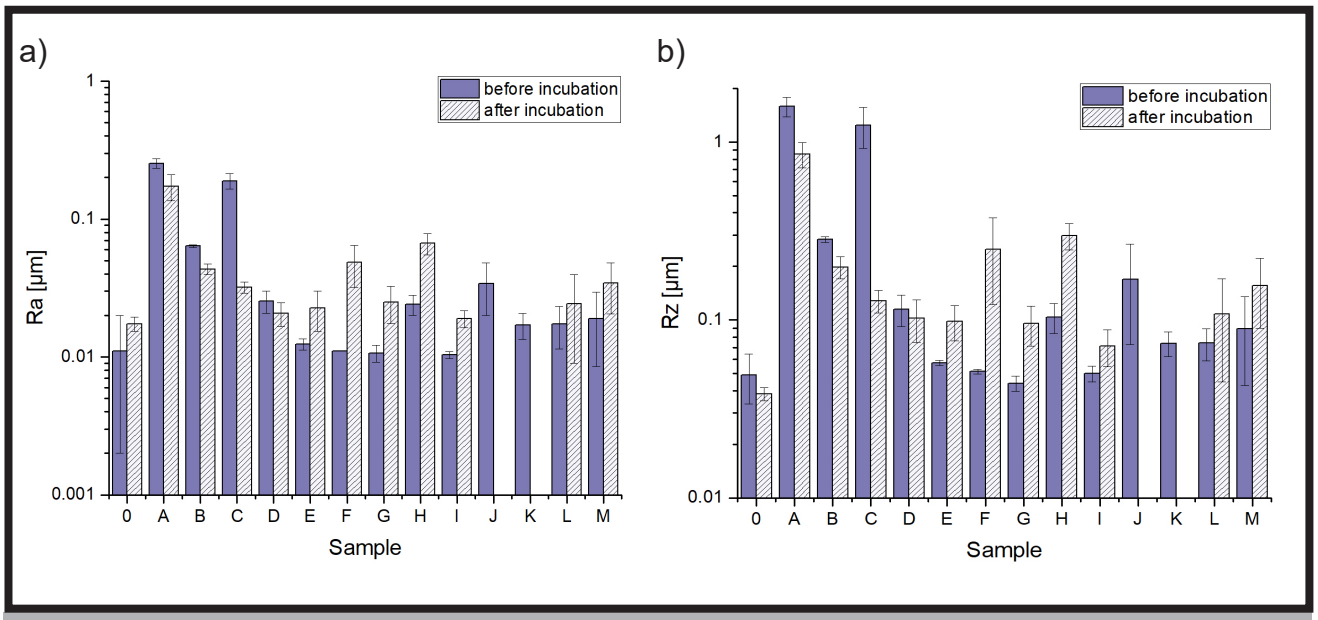

FIG. 4. The linear roughness values of the examined composites before and after incubation: a) Ra – arithmetic mean roughness, b) Rz – maximum height.

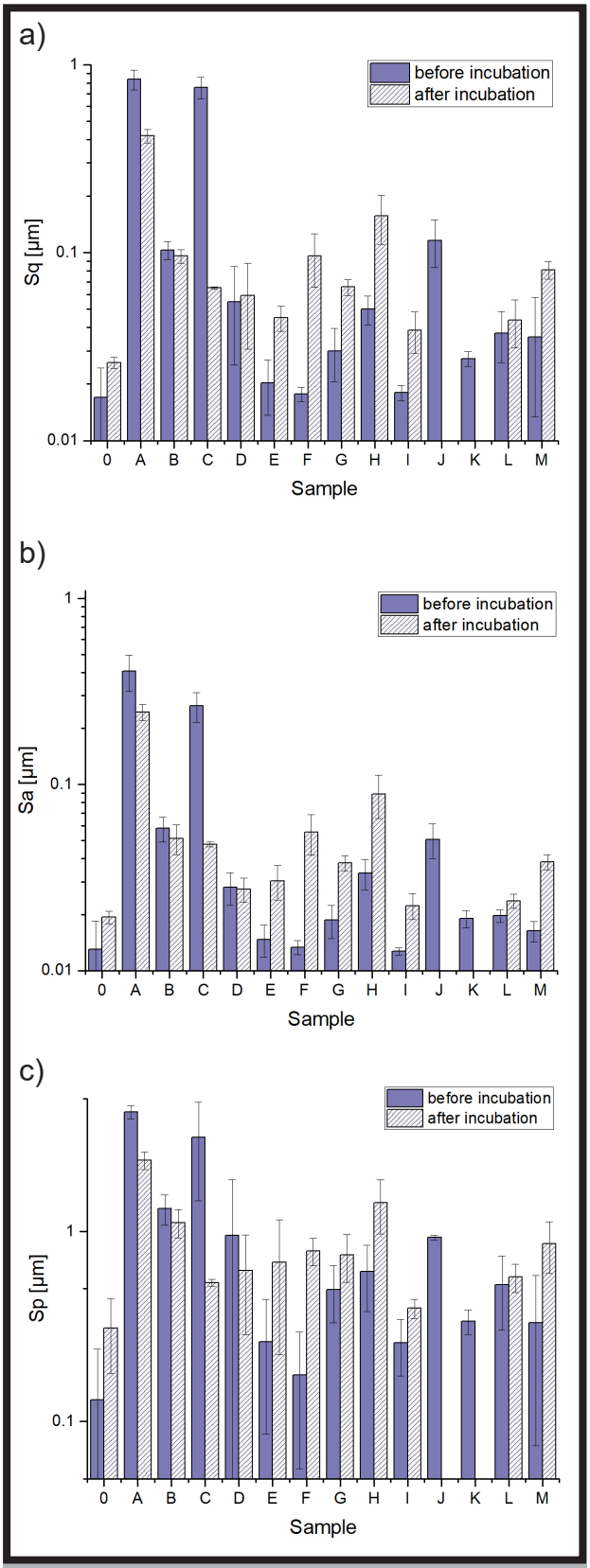

FIG. 5. Surface roughness parameters of the examined composites before and after incubation: a) Sq – root mean square height, b) Sa – arithmetical mean height, c) Sp – maximum peak height.

In FIG. 5 results for Sq, Sa, and Sp surface roughness parameters are presented. Generally, the Sq value was lower than 0.2 µm for the measured samples and tends to increase after the incubation process. The surface roughness was the highest for the non-silanized sample (A) (0.85 µm before and 0.42 µm after silanization) and the sample (C) after combined silanization and phosphorylation process (0.76 µm before incubation).

The Sa surface roughness increased for incubated composites in most of the cases. The difference between non-incubated and incubated samples was in the range of 0.01-0.02 µm. The exceptions were observed for the non-silanized sample (0.41 µm before and 0.25 µm after silanization for sample A) and the sample after the combined silanization and phosphorylation process (0.26 µm before incubation for sample C), where the roughness decreased.

Similarly, as in previous cases, the Sp roughness was the highest for the sample (A) with non-silanized powder (4.26 µm before and 2.37 µm after silanization) and the sample (C) after the combined silanization and phosphorylation process (3.13 µm before incubation). The Sp roughness for pure silicone (0) is 0.13 µm before silanization and increases to 0.31 µm after incubation.

The roughness of the examined surfaces was found to be lower for composites based on silanized powder. However, it should be noted that the roughness increased after the incubation process. In summary, it can be stated that the use of the silanization process reduces surface roughness [28].

The CLSM observations were also used to calculate the surface and volume of structures protruding above the average profile line of the material on the samples' surface (FIG. 6). They are called peaks and pits because they are higher or lower than other points in their respective neighbourhoods. Both the area and the volume occupied by the structures protruding on the surface of the sample allow us to assess how far all peaks and pits protrude from the base surface. The total surface of the peaks and pits is significantly higher for sample (A) with non-silanized microparticles (32107 μm^2) than for samples with modified powder (B-M). In most cases, the peaks and pits surface were more than six times lower for silanized powder-based composites. For all composites, the surface of peaks and pits decreased after incubation.

The volume of structures protruding above the average profile line of the material surface is of the highest value for 0 sample (pure silicone) and composite A with non-silanized powder (before incubation), for which the values obtained were 16129 μm^3 and 18027 μm^3, respectively. The most significant difference was measured for samples F and G (7653 μm^3 and 2342 μm^3, respectively). This may be due to the deepening of already existing peaks and pits.

There is a strong correlation between the surface area and the volume of the peaks and pits. Due to the r-Pearson correlation of 0.871 for $p < 0.001$, the measured values are interconnected. However, for a better description of the surface, these two parameters should be analyzed to fully characterize the tested surface.

In FIGs. 7 and 8 representative CLSM images of two samples, with non-silanized micropowder (A) and with silanized micropowder (composite M), before and after incubation were presented. Some particle agglomerations in both materials were observed. However, it can be noticed that fewer agglomerates are present in sample M, based on the silanized magnetic powder, as compared to the composite with non-silanized powder.

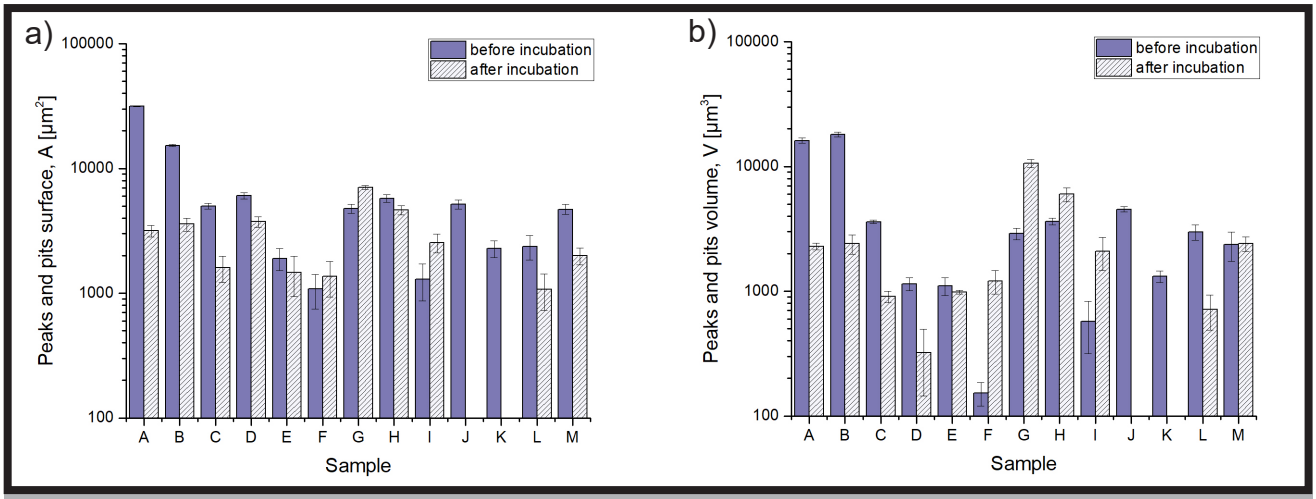

FIG. 6. a) Surface and b) volume of structures protruding above the average profile line of the surface in the examined composites before and after incubation.

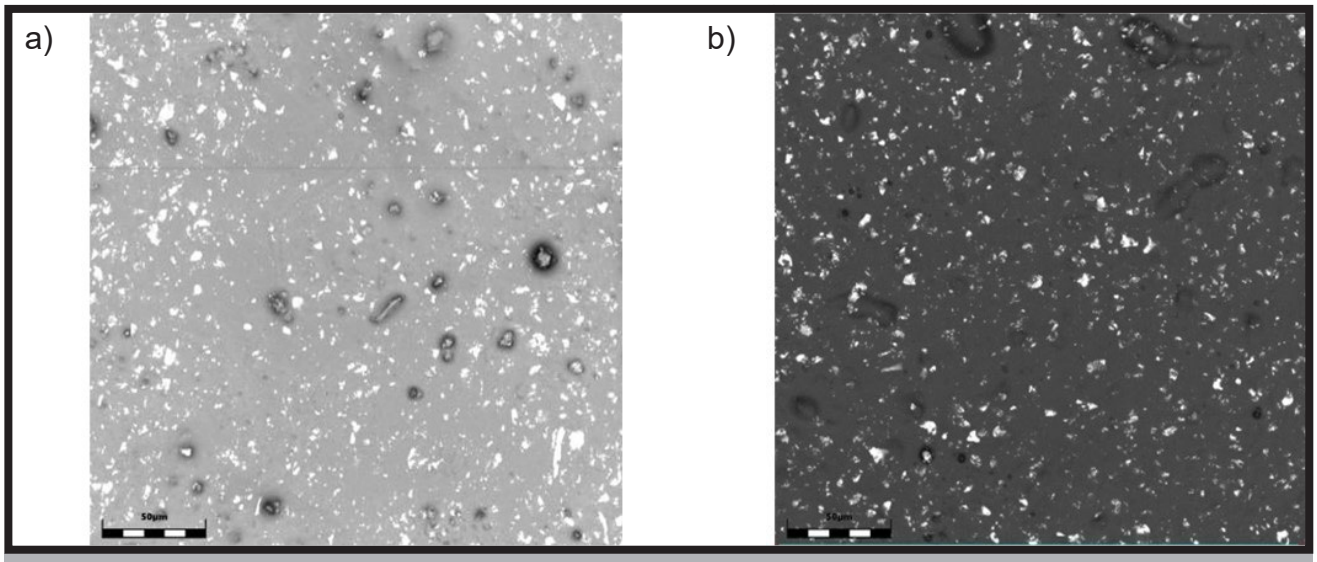

FIG. 7. The surface of composite with non-silanized micropowder a) before and b) after incubation. Scale bar 50 µm.

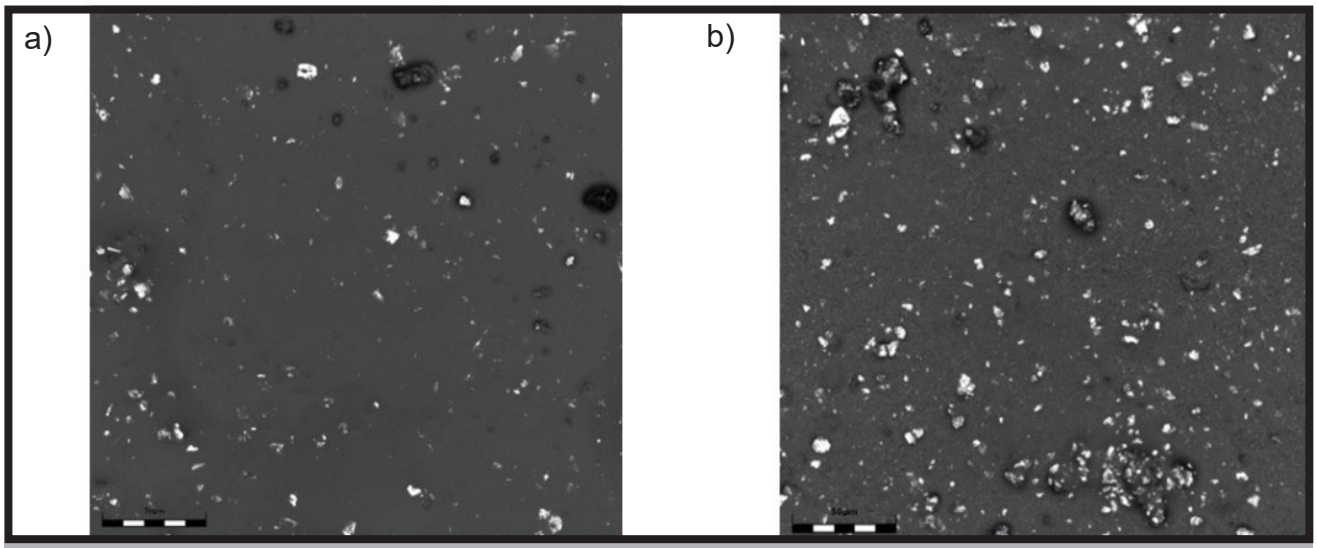

FIG. 8. The surface of composite with micropowder silanized with 7.5% APTES solution for 4 h, a) before and b) after incubation. Scale bar - 50 µm.

Conclusions

To enhance the bond between the magnetic powder and the organic matrix, the powder was silanized under different conditions. The appropriate selection of the silanization parameters allows for control of the properties of the composite. This is extremely important from the point of view of specific composite applications in biomedical engineering. Thus, in this study, variable parameters such as silane concentration, silanization time, and type of solution were examined. The obtained results show that the powder surface silanization affects the physicochemical and thermal stability of the prepared composites. Thermogravimetric analysis shows that the silanization process reduces the temperature of material's decomposition. It was also observed that the values of tested physicochemical properties were slightly higher for silanized powder-based composites. Surface roughness analysis results show that the composites with silanized powder (B-M, except for C) had significantly lower values of Ra, Rz, as well as Sq, Sa, and Sp parameters. Additionally, the silanization combined with phosphorylation presented in the literature as a promising method of modification, caused a worsening of tested composites properties, which are relevant for biomedical applications of the material. The obtained experimental results may lead to further research on the functionalization of composites based on magnetic powder.

Acknowledgements

This scientific work was realized in the frame of projects, No. WI/WM-IIB/3/2023 and WI/WM-IIB/5/2021 and financed from research funds of the Ministry of Education and Science, Poland.

ORCID iD

A. Powojska: https://orcid.org/0000-0003-3276-0592
J. Niewęgłowska: https://orcid.org/0000-0002-9035-7147
J. Mystkowska: https://orcid.org/0000-0002-3386-146X

References

[1] P.V. Mohanan, K. Rathinam: Biocompatibility studies on silicone rubber, in: Proc. First Reg. Conf. IEEE Eng. Med. Biol. Soc. 14th Conf. Biomed. Eng. Soc. India Int. Meet, IEEE, New Delhi, India, 1995: p. 4/11-4/12.
[2] D. Fallahi, H. Mirzadeh, M.T. Khorasani: Physical, mechanical, and biocompatibility evaluation of three different types of silicone rubber. J. Appl. Polym. Sci. 88 (2003) 2522-2529.
[3] J. Mystkowska, A. Powojska, D. Łysik, J. Niewęgłowska, G.S.C. Bermúdez, A. Mystkowski, D. Makarov: The Effect of Physiological Incubation on the Properties of Elastic Magnetic Composites for Soft Biomedical Sensors. Sensors 21 (2021) 7122.
[4] V. Iacovacci, G. Lucarini, C. Innocenti, N. Comisso, P. Dario, et al.: Polydimethylsiloxane films doped with NdFeB powder: magnetic characterization and potential applications in biomedical engineering and microrobotics. Biomed. Microdevices. 17 (2015) 112.
[5] Z. Wu, Q. Wang, J. Huang, Y. Yue, D. Chen, Y. Shi, B. Su: The soft NdFeB/Ecoflex composites for soft robot with a considerable magnetostimulated shrinkability, Compos. Sci. Technol. 217 (2022) 109129.
[6] V.E. Donohue, F. McDonald, R. Evans: In vitro cytotoxicity testing of neodymium-iron-boron magnets. J. Appl. Biomater. 6 (1995) 69-74.
[7] A. Powojska, J. Niewęgłowska, S. Suska, A. Cavadas, J. Mystkowska: Chemical stability assessment of soft magnetic composites for biomedical applications. Engineering of Biomaterials 164 (2022) 2-8.
[8] X. Zhang, Z. Wang, T. Li, S. Zhu, D. Yu, W. Yan, Y. Luo: Effect of silane coupling agents on flowability and compressibility of compound for bonded NdFeB magnet. J. Rare Earths. 40 (2022) 772-777.
[9] S.-B. Yeh, C.-S. Chen, W.-Y. Chen, C.-J. Huang: Modification of Silicone Elastomer with Zwitterionic Silane for Durable Antifouling Properties. Langmuir 30 (2014) 11386-11393.
[10] M. Zhu, M.Z. Lerum, W. Chen: How To Prepare Reproducible, Homogeneous, and Hydrolytically Stable Aminosilane-Derived Layers on Silica. Langmuir 28 (2012) 416-423.
[11] C. Velasco-Santos, A.L. Martinez-Hernandez, V.M. Castano: Silanization of Carbon Nanotubes: Surface Modification and Polymer Nanocomposites, in: S. Yellampalli (Ed.), Carbon Nanotub. - Polym. Nanocomposites, InTech, 2011.
[12] N. Aissaoui, L. Bergaoui, J. Landoulsi, J.-F. Lambert, S. Boujday: Silane Layers on Silicon Surfaces: Mechanism of Interaction, Stability, and Influence on Protein Adsorption. Langmuir 28 (2012) 656-665.
[13] S. Villa, P. Riani, F. Locardi, F. Canepa: Functionalization of Fe_3O_4 NPs by Silanization: Use of Amine (APTES) and Thiol (MPTMS) Silanes and Their Physical Characterization. Materials 9 (2016) 826.
[14] B. Qiao, T.-J. Wang, H. Gao, Y. Jin: High density silanization of nano-silica particles using γ-aminopropyltriethoxysilane (APTES). Appl. Surf. Sci. 351 (2015) 646-654.
[15] Z. Liao, J. Yang, M. Hossain, G. Chagnon, L. Jing, X. Yao: On the stress recovery behaviour of Ecoflex silicone rubbers. Int. J. Mech. Sci. 206 (2021) 106624.
[16] ISO 10993-13:2010 Biological evaluation of medical devices Part 13: Identification and quantification of degradation products from polymeric medical devices.
[17] ISO 11358-1:2022 Plastics Thermogravimetry (TG) of polymers Part 1: General principles.
[18] J. López-Cuevas, M.I. Pech-Canul, J.L. Rodríguez-Galicia, J.C. Rendón-Angeles: A Practical Procedure for Measuring Contact Angles in Wettability Studies by the Sessile Drop Method. MRS Adv. 4 (2019) 3143-3152.
[19] T. Zhao, L. Jiang: Contact angle measurement of natural materials, Colloids Surf. B Biointerfaces. 161 (2018) 324-330.
[20] W. Moon, J.H. Park, H.-A. Lee, B.-S. Lim, S.H. Chung: Influence of Additive Firing on the Surface Characteristics, Streptococcus mutans Viability and Optical Properties of Zirconia. Materials 14 (2021) 1286.
[21] D. Sun, H. Shang, H. Jiang: Effective metrology and standard of the surface roughness of micro/nanoscale waveguides with confocal laser scanning microscopy. Opt. Lett. 44 (2019) 747.
[22] A. Kaidarova, M.A. Khan, S. Amara, N.R. Geraldi, M.A. Karimi, A. Shamim, R.P. Wilson, C.M. Duarte, J. Kosel: Tunable, Flexible Composite Magnets for Marine Monitoring Applications. Adv. Eng. Mater. 20 (2018) 1800229.
[23] M. Qin, S. Hou, L. Wang, X. Feng, R. Wang, Y. Yang, C. Wang, L. Yu, B. Shao, M. Qiao: Two methods for glass surface modification and their application in protein immobilization. Colloids Surf. B Biointerfaces 60 (2007) 243-249.
[24] K. Wang, G. Wang, C. Lu: Particle contact angle at the oil-water interface: Effect of surface silanization. Particuology 44 (2019) 218-224.
[25] M.W. Cowle, G. Webster, A.O. Babatunde, B.N. Bockelmann--Evans, A.J. Weightman: Impact of flow hydrodynamics and pipe material properties on biofilm development within drinking water systems. Environ. Technol. 41 (2020) 3732-3744.
[26] B.R. Prasad, M.A. Brook, T. Smith, S. Zhao, Y. Chen, H. Sheardown, R. D'souza, Y. Rochev: Controlling cellular activity by manipulating silicone surface roughness, Colloids Surf. B Biointerfaces 78 (2010) 237-242.
[27] A. Al-Ani, H. Pingle, N.P. Reynolds, P.-Y. Wang, P. Kingshott: Tuning the Density of Poly(ethylene glycol) Chains to Control Mammalian Cell and Bacterial Attachment. Polymers 9 (2017) 343.
[28] D. Lee, S. Yang: Surface modification of PDMS by atmospheric-pressure plasma-enhanced chemical vapor deposition and analysis of long-lasting surface hydrophilicity. Sens. Actuators B Chem. 162 (2012) 425-434.

PHYSICAL PROPERTIES OF BIODEGRADABLE POLYMERS EXPOSED TO ARTIFICIAL PLASMA FLOW

Alicja Zegartowska[1]*, Mateusz Stojko[2], Kamil Joszko[1], Karolina Goldsztajn[1], Ada Orłowska[1], Janusz Szewczenko[1]

[1] Faculty of Biomedical Engineering,
Silesian University of Technology,
Franklina Roosevelta 40,
41-800 Zabrze, Poland
[2] Centre of Polymer and Carbon Materials,
Polish Academy of Sciences,
M. Curie-Sklodowskiej 34,
41-819 Zabrze, Poland
*e-mail: aliczeg420@student.polsl.pl

Abstract

Despite significant advances in diagnosis and treatment, cardiovascular disease remains a major cause of premature death. Approximately 80% of cardiovascular incidents can be prevented by optimizing risk factor control and lifestyle modification, including dietary change. Treatment of cardiovascular disease, like treatment of other diseases, can be divided into conservative and curative. Conservative treatment is based on pharmacotherapy, while surgical treatment is mainly based on the use of PCI (percutaneous coronary intervention) procedures, i.e., increasing blood flow through narrowed arteries. This effect can be achieved with stents. The main limitation of metal stents is their permanent presence within the body, which can lead to complications such as thrombosis. A more advanced solution is the use of polymer or drug-coated stents, both of which are made of biodegradable materials. These stents are designed to release medications to support treatment and maintain their shape within the blood vessel before being naturally absorbed and eliminated by the body. In this study, the surface of stents made of polylactide was modified by applying a layer of PLGA using an ultrasound method. The study was carried out for uncoated and coated stents in both the initial state and after exposure to artificial plasma flow. The scope of the work included microscopic observations, weight measurements of the specimen, and examination of radial forces. The analysis of the results showed no clear effect of exposure on stent weight, but a clear effect of long--term exposure on radial forces was observed.

Keywords: *bioresorbable stents, biodegradable coating, poly(L-lactide-co-glycolide) (PLGA), splay coating, radial forces*

[Engineering of Biomaterials 170 (2023) 9-13]

doi:10.34821/eng.biomat.170.2023.9-13

Submitted: 2023-09-01, Accepted: 2023-09-27, Published: 2023-09-30

Introduction

Cardiovascular diseases are the leading cause of death worldwide. According to the WHO (World Health Organization), these diseases take the lives of approximately 17.9 million people each year. They belong to a group of cardiovascular disorders that includes diseases such as ischemic heart disease, vascular restenosis, cerebrovascular disease, and other conditions. Risk factors are social and cultural changes, including low physical activity, poor diet, stress, and smoking or consuming harmful amounts of alcohol [1].

The treatment of cardiovascular disease depends on the severity of the disease and the risk to the patient. If the cause of the disease is excessively high cholesterol levels that affect the quality of blood flow or irregular heart rhythm, pharmacological treatment is implemented. The pharmacological treatment of cardiovascular diseases depends mainly on the specific disease entity with which the patient is struggling. In the case of hypertension, hypotensive drugs are used; in the case of heart failure, multidrug therapy is used to modify the cause as much as possible. The more advanced form of the disease associated with partial or complete blockage of a blood vessel is surgically treated with coronary angioplasty or coronary artery bypass grafting. Coronary angioplasty is a procedure used to unblock the arteries of the heart using a small balloon catheter that is inserted into the blocked blood vessel to dilate it. Angioplasty is often combined with the placement of a small wire mesh tube called a stent. The use of angioplasty along with stenting has many advantages for the patient; in some cases, it can eliminate the need for arterial bypass surgery, which is a more invasive procedure and is also associated with a prolonged recovery time [2,3].

A stent is a medical implant that is used to maintain the normal shape of the arteries affected by atherosclerosis and prevent them from narrowing again. A stent looks like a cylinder with a diameter of approximately 3-8 mm and a thin mesh structure of 150-200 microns thick. Depending on the characteristics of the disease and the function of the vascular prosthesis, we can distinguish different types of stents. Concerning the method of implantation, stents can be divided into classic BMS (bare-metal stent) stents, also referred to as metal stent-grafts, in which it is first necessary to dilate the blood vessels using a catheter. Self-expandable stents, which are characterized by variable expansion force, thus reducing the risk of various complications such as stent thrombosis. Another classification of stents is based on the material used to manufacture them. A distinction is made between metal stents, bioresorbable stents, and the latest generation of drug-eluting stents (DES). Metal stents are usually made of alloys containing elements such as chromium or vanadium, for example, cobalt-chromium or nickel-titanium. Their negative influence related to metal-organ interaction and restenosis has prompted the development of research into bioresorbable stents, which are made of materials such as aliphatic polyesters and polyacids. These materials meet all the requirements for interaction with the human body, i.e. low toxicity, degradability under biological conditions, and adequate mechanical strength. In addition, these materials are largely amorphous, which facilitates their uniform degradation. Bioresorbable stents dissolve completely a few months after implantation. After this period, the treated vessel segment regains physiological function. Therefore, the potential benefit of bioresorbable stents is the prospect of long-term restoration of vascular endothelial reactivity and vascular reconstruction in just a few months.

Complete biodegradation eliminates the risk of late adverse coronary incidents related to the presence of foreign bodies in the vessel. The latest generation of drug-eluting DES stents is characterized by the release of specific drugs such as sirolimus and everolimus. These reduce the process of restenosis, i.e. the overgrowth of the vessel lumen [4-8].

The choice of stent type should be based on detailed clinical data and take into account: clinical indications; the presence of comorbidities, including those requiring chronic anticoagulation; the risk of bleeding associated with prolonged dual antiplatelet therapy; the risk of premature discontinuation of antiplatelet therapy (medical contraindications, patient non-cooperation). A significant advance in the field of vascular prostheses has been the use of polymer coatings as a matrix for the release of therapeutic substances. Polymer-coated stents, unlike classic metal stents, exhibit high plasticity, facilitating the transfer of the prosthesis to the target implantation site, and the polymer coating provides a good matrix for immobilization and controlled release of antiproliferative drugs. Therefore, implants of this type are an interesting alternative in the treatment of coronary artery disease. The undoubted advantage of using this type of stent is its biocompatibility (rapid and proper formation of neointima) without the need for long-term dual antiplatelet therapy [9-12].

The study aimed to determine the physical properties of biodegradable polymer stents covered with a PLGA coating. Long-term studies of exposing stents to the flow of artificial plasma were performed for stents with and without coating.

Materials and Methods

Stents with a length of 10 mm and a diameter of 3 mm made of modified polylactide using the microinjection method (FIG. 1) were obtained from the Center of Polymer and Carbon Materials of the Polish Academy of Sciences in Zabrze. They were divided into two groups, i.e. 14 stents remained in the initial state, while 12 stents were coated with seven layers of poly(L-lactide-co-glycolide) (PLGA), each layer applied with the same parameters [7]. The application of coatings on the stents was performed using the ExtraCoat (Sono-Tech, USA) ultrasonic coating system, with the parameters shown in TABLE 1. 2% solution of PLGA in dichloromethane was used in the coating process.

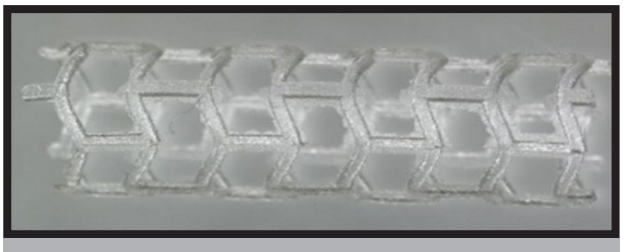

FIG. 1. Stent in the initial state.

TABLE 1. Parameters of the coating system.

Ultrasound frequency	60 kHz
Ultrasound power	1.5 W
Solution flow rate	0.5 cm^3/min
Sliding speed	5 mm/s
Air curtain pressure	3 Pa
Time between successive coats	15 s

After the application process was completed, the stents were dried for 48 h under ambient conditions and then for the next 24 h in a laboratory dryer at 30ºC.

The stents were exposed to artificial plasma flow for 1, 14 and 28 days. In each trial, 3 uncoated stents and 3 stents with a polymer coating were used. The tests were carried out in artificial plasma at a temperature of 36.6ºC in the range of pressure changes of 80-120 mmHg and a flow rate of 1.1 m/s. Plasma flow in a single tube was 15 ml/s. Artificial plasma with the content of: 0.14 M NaCl, 0.0027 M KCl, and 0.01 M PO_4^{3-} (Chemsolve) was used in the research.

In the work, for stents without and with a polymer coating before and after exposure to the flow of artificial plasma, the following study was carried out.

The weight of the samples was determined using the analytical scale RADWAG AS 310.R2, with an accuracy of 0.0001 g. Microscopic observations of the stents were made using a Leica DVM6 digital microscope. The radial force test was carried out at the Center for Polymer and Carbon Materials of the Polish Academy of Sciences using the TTR2 with the J-Crimp Blockwise radial force testing system, which enables the testing of stents with various design features. Before measurements, the stents were conditioned at 37ºC for 30 s. The tests were performed with the parameters presented in TABLE 2.

TABLE 2. Parameters of the radial force test.

Starting diameter	3 mm
Final diameter	1.5 mm
Clamping speed	0.5 mm/s
Measurement temperature	37ºC

Results and Discussions

The mean values and standard deviations of the weight of uncoated (U) and polymer-coated (C) stents after different times of exposure to the flow of artificial plasma are presented in TABLE 3.

TABLE 3. Summary of weight of coated (C) and uncoated (U) stents after exposure.

Time of exposure [day]	Stent	Average stent weight [mg]
0	U	4.00 ± 0.38
	C	4.60 ± 0.35
1	U	4.30 ± 0.60
	C	4.50 ± 0.10
14	U	4.30 ± 0.20
	C	4.80 ± 0.10
28	U	4.00 ± 0.12
	C	4.10 ± 0.50

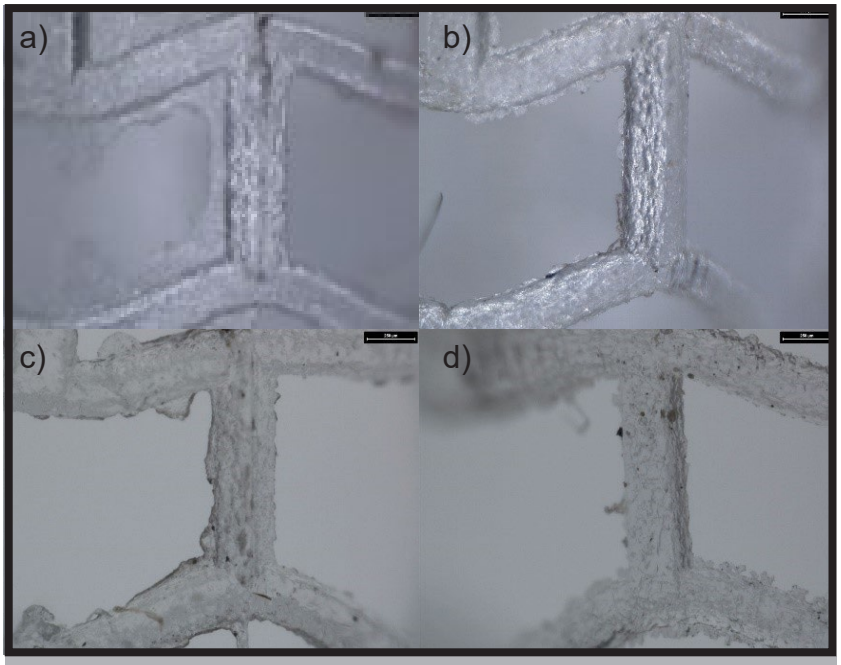

FIG. 2. Stents in initial state: (a, b) uncoated, (c, d) polymer-coated.

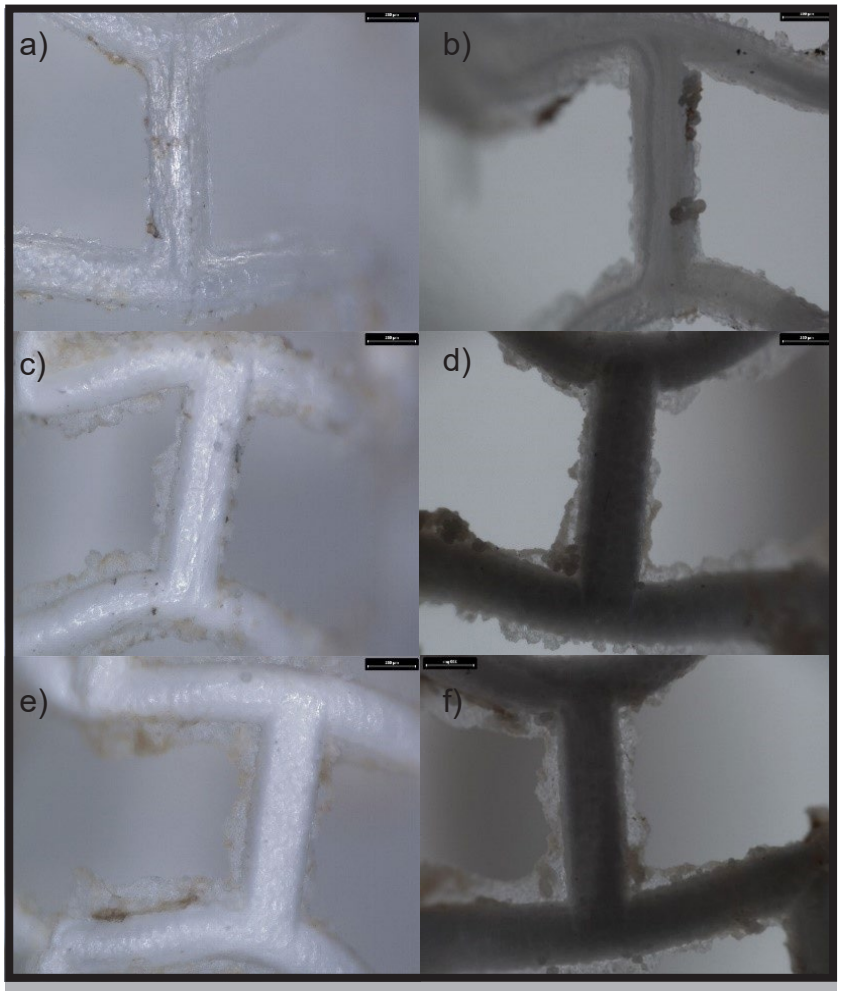

FIG. 3. Uncoated stent exposed to artificial plasma flow for: (a, b) 1 day, (c, d) 14 days, (e, f) 28 days.

The results of the stent weight in the initial state range from 4 mg to 5 mg. These differences result from the accuracy of the stent manufacturing process using the microinjection method, as well as the accuracy of stent trimming. The weight of the stents after exposure to plasma flow increased by an average of 0.6 mg compared to the stents before exposure. The increase in the weight of the stent after exposure is due to the deposition components of artificial plasma in the form of crystals on the stent, as well as the swelling of the polymer. Measurement of the mass of the stents in their original and coated states after exposure to plasma flow did not show significant differences.

Stents without and with coating before and after exposure to artificial flow plasma are shown in FIGs 2, 3 and 4.

The analysis of microscopic observations of the sample in the initial state revealed a smooth surface of the stent with visible sprues being the remnants of the stent manufacturing process (FIG. 2a, b). The application of the polymer coating caused the surface of the stent to become heterogeneous and characterized by greater surface development compared to the stent without the coating (FIG. 2c, d).

Microscopic observations of the stents in the initial state (FIG. 3) and with coating (FIG. 4) after different times of exposure to the plasma flow revealed additional deposits on the stent spans and sprues. The deposits in the form of crystals are the remains of the components of artificial plasma. The number of observed crystals increased with exposure time. A greater number of crystals was observed on the coated stents.

In the stents exposed to the flow of artificial plasma, after the radial forces tests (FIG. 5), changes in the shape (approach of the spans - FIG. 5b) and the places of rip stent tearing located in the zone span connections (FIG. 5a) were observed. The observations also confirmed that the presence of sprues after the stent manufacturing process and deposits in the form of crystals are the remains of the components of artificial plasma. These observations refer to both uncoated and coated stents.

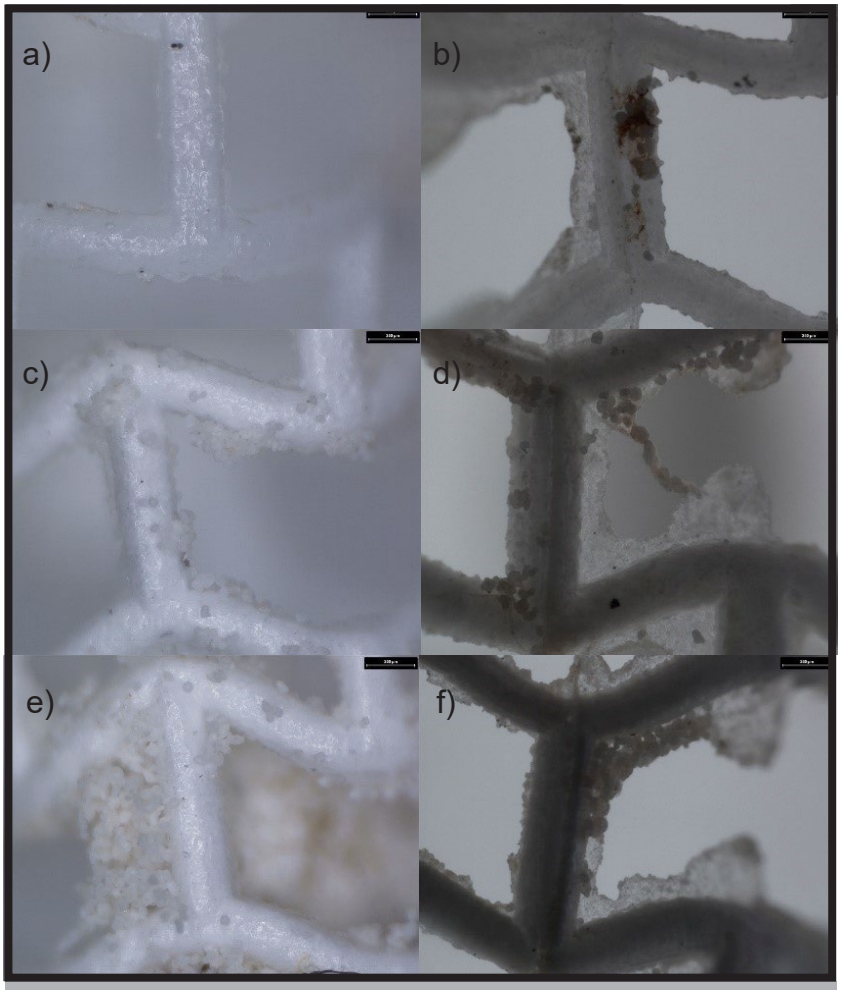

FIG. 4. Polymer-coated stent exposed to artificial plasma flow for: (a, b) 1 day, (c, d) 14 days, (e, f) 28 days.

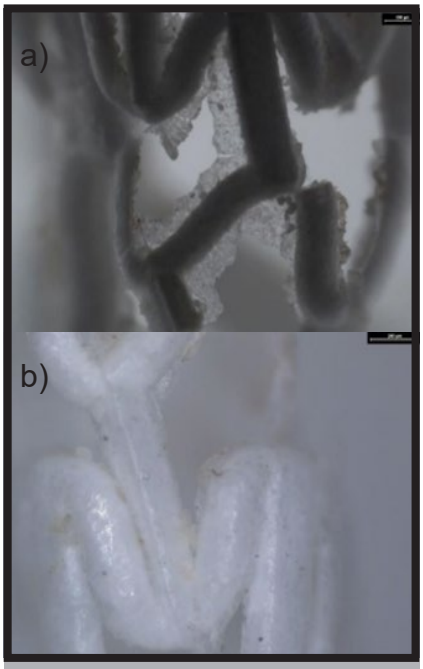

FIG. 5. Stents exposed to artificial plasma flow and then subjected to radial force tests: a) uncoated, b) coated.

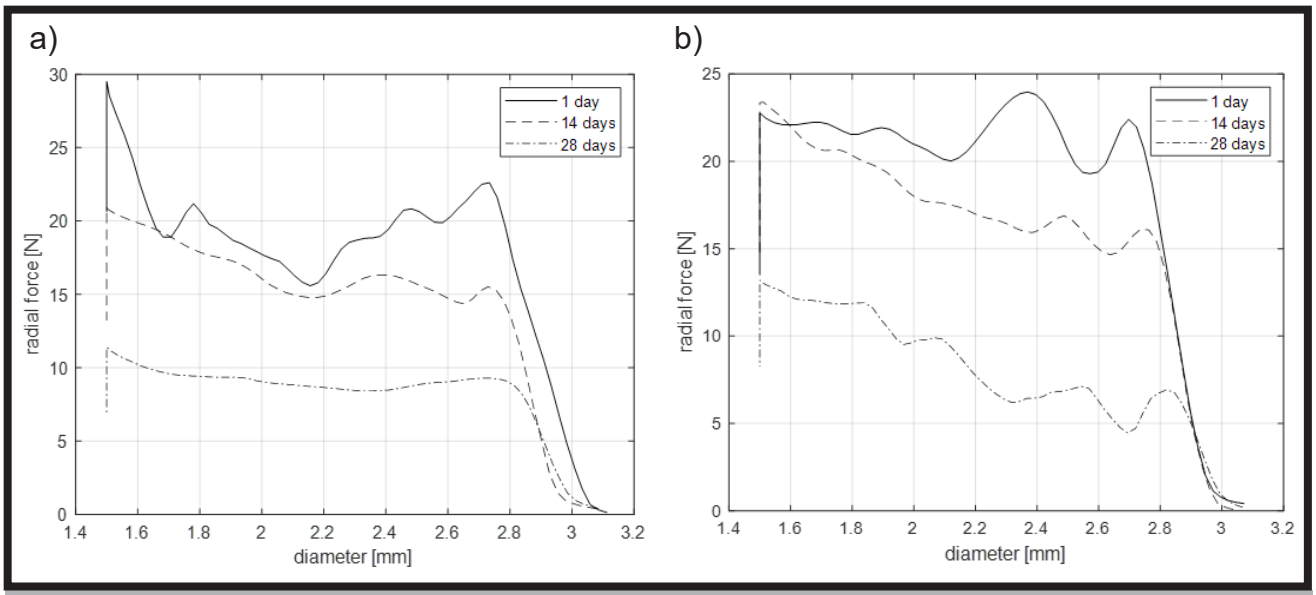

FIG. 6. Example characteristics obtained during radial strength tests of stents after different exposure times to artificial plasma flow: a) uncoated stents, b) coated stents.

Examples of radial force versus stent diameter curves from studies of the radial strength of the stents (without and with a polymer coating) and earlier exposure to a flow of artificial plasma are shown in FIG. 6. Curves showing the changes in radial force as a function of the stent diameter are characterized by a heterogeneous course. Along the curves, we can distinguish the elastic range, followed by plastic deformation of the material, ending with its breaking. With increasing exposure time to artificial plasma flow, a decrease in the radial force of the stents was observed. Moreover, it was observed that as the exposure time of the stents increased, the range of plastic deformations increased and the force at which the stent was destroyed decreased. For stents after 28 days of exposure, the smallest impact of changing the stent diameter on the value of its radial force was observed. A similar course of radial force curves as a function of stent diameter for different times of exposure to the flow of artificial plasma was observed for stents without and with a polymer coating.

Analysis of the test results of the radial force value at which damage occurred in stents exposed for a longer time to artificial plasma flow (14, 28 days) did not show significant differences between stents with and without a PLGA coating (TABLE 4). The higher value of the radial force was in the initial state (0) and after 1 day of exposure to plasma flow; uncoated stents (U) were compared to coated stents (C). Regardless of the type of the stent, it was observed that as the exposure time to plasma flow increased, the radial force at which the stent was damaged decreased.

TABLE 4. Radial destructive force for the uncoated (U) and coated (C) stents, exposed for different times to the flow of artificial plasma.

Time of exposure [days]	Stent	Radial destructive force value [N]
0	U	17.4 ± 4.6
	C	19.5 ± 4.9
1	U	20.9 ± 5.5
	C	19.1 ± 5.7
14	U	17.7 ± 5.3
	C	17.5 ± 5.2
28	U	8.6 ± 2.2
	C	8.3 ± 3.2

Conclusions

To summarize:

- the surface of the PLGA spray-coated stent is heterogeneous and characterized by a greater surface development as compared to the stent without the coating;
- no effect of PLGA coating on the change in weight of the stent exposed to the flow of artificial plasma was observed, for both coated and uncoated stents, the observed temporal weight changes were similar and unambiguous;
- the PLGA coating does not affect the radial strength of the stent, both in the case of the stents with and without the coating, the decrease in the radial force with increasing exposure time to the flow of artificial plasma was noted;
- the weight of the stents after exposure to plasma flow increased by an average of 0.6 mg compared to the stents before exposure. The increase in the weight of the stent after exposure is due to the deposition components of artificial plasma in the form of crystals on the stent, as well as the swelling of the polymer;
- measurement of the mass of stents in their original and coated states after exposure to plasma flow did not show significant differences.

The analysis of the study results shows the suitability of the ultrasound method for the application of polymer coatings on biodegradable vascular stents. The produced PLGA coating does not change the mechanical properties of the stent in its initial state or after exposure to artificial plasma flow. This indicates the possibility of using such a coating as a matrix for locally released active substances.

Acknowledgements

The study was conducted in the frame of project of the National Centre for Research and Development no. POIR.04.01.02-00-0105/17 – MICROINJSTENT.

ORCID iD

A. Zegartowska: https://orcid.org/0009-0000-7552-8617
M. Stojko: https://orcid.org/0000-0001-8868-9495
K. Joszko: https://orcid.org/0000-0002-8229-3032
K. Goldsztajn: https://orcid.org/0000-0003-2545-9339
A. Orłowska: https://orcid.org/0000-0002-0168-7508
J. Szewczenko: https://orcid.org/0000-0001-9718-8617

References

[1] https://www.who.int/health-topics/cardiovascular-diseases#tab=tab_1
[2] F. Otsuka, M. Nakano, F.D. Kolodgie, R. Virmani: Evaluation of Vulnerable Atherosclerotic Plaques. In: Coronary Artery Disease; Eds. T.J. Willerson, J.R.D. Holmes; Springer, London 2015.
[3] B.J. Bachar, B. Manna: Coronary Artery Bypass Graft, National Library of Medicine, In: StatPearls. Treasure Island (FL): StatPearls Publishing 2023.
[4] A. Guildford, M. Santin, G.J. Phillips: Cardiovascular stents. In: Biomaterials and Devices for the Circulatory System, University of Brighton, Woodhead Publishing Series in Biomaterials (2010) 173-216.
[5] J. Marciniak: Stenty w chirurgii małoinwazyjnej, wyd. Politechniki Śląskiej, Gliwice 2006
[6] M. Latos, A. Masek: Biodegradowalne poliestry. Instytut Technologii Polimerów i Barwników, Łódź 2017
[7] I. Vroman, L. Tighzert: Biodegradable Polymers. Materials 2(2) (2009) 307-344.
[8] H. Ding, Y. Zhang, Y. Liu, C. Shi, Z. Nie, H. Liu, Y. Gu: Analysis of Vascular Mechanical Characteristics after Coronary Degradable Stent Implantation. BioMed Research Interational (2019) 8265374.
[9] R.C. Eberhart, S.-H. Su, K.T. Nguyen, M. Zilberman, L. Tang, K.D. Nelson, P. Frenkel: Bioresorbable polymeric stents: current status and future promise. Journal of Biomaterials Science, Polymer Edition 14(4) (2003) 299-312.
[10] A. Foerster, M. Duda, H. Kraśkiewicz, M. Wawrzyńska, H. Podbielska, M. Kopaczyńska: Physico-chemical stent surface modifications. In: Functionalised Cardiovascular Stents, Eds. J.G. Wall, H. Podbielska, M. Wawrzyńska, Woodhead Publishing (2018) 137-148.
[11] M.A. Sayed Patwary, S.M. Surid, M.A. Gafur: Properties and Applications of Biodegradable Polymers. Journal of Research Updates in Polymer Science 9 (2020) 32-41.
[12] E. Vassallo, M. Pedroni, M. Aloisio, S.M. Pietralunga, R. Donnini, F. Saitta, D. Fessas: Plasma Treatment of Different Biodegradable Polymers: A Method to Enhanc Wettability and Adhesion Properties for Use in Industrial Packaging. Plasma 7(1) (2024) 91-105.

MESENCHYMAL STEM CELLS PROLIFERATION AND OSTEOGENIC DIFFERENTIATION ON POLYMERIC SCAFFOLDS AND MICROSPHERES FOR BONE TISSUE ENGINEERING

Kamila Walczak*, Małgorzata Krok-Borkowicz, Elżbieta Pamuła

AGH University of Krakow,
Faculty of Materials Science and Ceramics,
Department of Biomaterials and Composites,
al. A. Mickiewicza 30, 30-059 Krakow, Poland
*e-mail: kamwalczak@agh.edu.pl

Abstract

In this study, we aimed to compare how the microstructure and architecture of polymer supports influence adhesion, growth and differentiation of human mesenchymal stem cells (hMSC) in the context of bone tissue engineering. We manufactured poly(L-lactide-co-glycolide) (PLGA) three-dimensional supports in the form of microspheres by emulsification and porous scaffolds by solvent casting/porogen leaching. HMSC were seeded on both materials and on control tissue culture polystyrene (TCPS, bottom of the wells) and cultured in basal or osteogenic medium for 1, 3, 7 and 14 days. HMSC proliferation and osteogenic differentiation were studied using lactate dehydrogenase (LDH) and alkaline phosphatase (ALP) assays, respectively. Furthermore, cell morphology and viability were analyzed after live/dead fluorescence staining. The results show that the optimized emulsification conditions allowed the production of PLGA microspheres with a median size of 95 µm. The PLGA scaffolds had a porosity of 82.1% ± 4.2% and a pore size of 360 µm ± 74 µm. HMSC cultured on control TCPS in osteogenic medium were more spread and polygonal than those in basal medium. They were characterized with a lower proliferation rate, as shown by the LDH results, but higher ALP activity. This suggests that hMSC osteogenic differentiation was achieved. The same tendency was observed for cells cultured on microspheres and scaffolds. Cell proliferation was more efficient on both materials and control in growth medium as compared to differentiation medium. The amount of ALP, i.e. a marker of osteogenic differentiation, was elevated, as expected, in differentiation medium. However, on day 14 cells cultured on the scaffolds in basal medium exhibited the same osteogenic potential as those cultured in differentiation medium. In general, both microspheres and scaffolds promoted hMSC adhesion, proliferation, and osteogenic differentiation and may be used for bone tissue engineering.

Keywords: *bone tissue engineering, scaffold, microspheres, proliferation, osteogenic differentiation*

[Engineering of Biomaterials 170 (2023) 14-19]

doi:10.34821/eng.biomat.170.2023.14-19

Submitted: 2023-08-30, Accepted: 2023-09-28, Published: 2023-10-01

Introduction

Bone is a highly specialized tissue, which, due to its structure, can be called a natural polymer-ceramic composite [1,2]. Bone tissue consists of living cells embedded in a matrix that comprises 30% organic substances (collagen, proteins, lipids, proteoglycans, osteopontin) and 70% inorganic substances (mainly hexagonal hydroxyapatite, arranged parallel to the long axis of collagen fibers) [1].

In terms of regeneration, bone tissue is unique because it undergoes complete and continuous regeneration without scarring. Bone trauma is the most common factor inducing the cascade of repair processes. The process of bone tissue regeneration can be divided into three phases: inflammation, bony callus formation, and bone remodelling [1,3]. During that process, the structural composition, cellular composition and biomechanical functions of the pre-injury tissue can be practically completely restored. Nevertheless, there is a small percentage of injuries when healing does not occur as expected. This applies mainly to extensive injuries whose volume exceeds the size of the critical defect. These types of injuries usually require surgical intervention.

Poly(L-lactide-*co*-glycolide) (PLGA) is a linear copolymer of L-lactide and glycolide. It degrades to lactic acid and glycolic acid, which at higher concentrations are cytotoxic. It is possible to regulate the rate of degradation of PLGA by changing the percentage of each monomer. As a rule, the degradation time is in the range of several weeks to several months [4,5]. This material is commonly used in tissue engineering due to its ease of processing, excellent biocompatibility, good mechanical performance, and degradability.

Scaffolds are three-dimensional porous structures that are permeable to cells and designed for temporary contact with tissues [6,7]. An ideal scaffold should be biocompatible and biodegradable. Over time, the scaffolds should degrade, thus giving space for cells to continue their growth. Scaffolds should provide a space in which the formation of new tissue, neovascularization, or remodelling of the regenerated structure can take place, with the aim of integrating it into the patient's tissues. Several conditions regarding the architecture of scaffolds are necessary for the above-described phenomenon to take place. First of all, the pores should be interconnected so that the diffusion of oxygen and nutrients into the cells and the diffusion of metabolites from the cells is possible [8]. Porosity contributes to better adhesion and migration of cells into the scaffold. To do this, scaffolds should imitate the mechanical conditions and natural bone structures that encourage cell differentiation into the desired phenotype. The optimal porosity is supposed to be within the range of 60% and 90%. Ideally, they would include a degree of micropores with sizes less than 10 µm to promote cell-scaffold interactions and micropores with diameters close to 300 µm to support osteogenesis [7].

Microspheres can be described as small spherical particles (from 1 µm to 1000 µm) that have the ability to move freely [9]. Their main advantage is that they have a relatively large surface area with a small volume, which is why they have quickly become popular in medicine as drug carriers or cell culture substrates [10]. Due to this feature, they provide better access to nutrients and oxygen and at the same time assure efficient metabolic waste removal. Moreover, since microspheres are regarded as 3D constructs, they provide an environment similar to natural conditions in which cells proliferate in living organisms [11].

Another advantage is that there are a large number of methods of obtaining microspheres such as emulsification, coacervation, or phase separation [10]. Mielan et al. obtained PLGA microspheres with an average diameter of 165 ± 47 μm. Their research proved that human mesenchymal stem cells (hMSC) proliferated and differentiated towards the osteogenic lineage successfully when cultured on PLGA microspheres [12].

The aim of this research was to fabricate 3D supports made of PLGA in the form of microspheres and scaffolds and to seed on them hMSC in order to access their adhesion, proliferation, and osteogenic differentiation. The outcome provided information concerning the potential of these materials in bone tissue defect healing, which allows us to assess the effectiveness of 3D supports. To the best of our knowledge, the comparison of PLGA scaffolds and microspheres in the context of MSC growth and osteogenic differentiation has not previously been described.

Materials and Methods

Microspheres fabrication

Poly(L-lactide-*co*-glycolide) (PLGA, 85% L-lactide, 15% glycolide, synthesized in the Polish Academy of Sciences, Zabrze, Poland), poly(vinyl alcohol) (PVA, Mowiol, M_w = 31,000 g/mol, Sigma Aldrich), and dichloromethane (DCM, PureLan, 99.7%) were used in this study. Microspheres were obtained using the emulsion method with solvent evaporation. The first step was to prepare a 1% PVA solution by dissolving 10.2 g of PVA in 1000 ml of distilled water. In order to obtain a homogeneous solution, it was placed on a magnetic stirrer (Jeio Tech, Multi-Channel Stirrer, MS-52M) at a speed of 400 rpm for 24 h. At the same time, a PLGA solution was prepared by dissolving 1.2 g of PLGA in 30 ml of dichloromethane (DCM). The prepared solution was placed on a magnetic stirrer (400 rpm) for 24 h.

After this time, 50 ml of the previously prepared PVA solution was poured into each of 10 beakers and 3 ml of PLGA solution was added dropwise using an automatic pipette. The beakers were then placed on a magnetic stirrer (400 rpm) for another 24 h. Stirrers of the same size were placed in the beakers so that the movement generated by them was comparable in each beaker. After the solvent (DCM) had completely evaporated and spherical microspheres could be clearly seen in the beakers, they were filtered through filter paper under pressure and rinsed with distilled water. As a next step, the papers with microspheres were placed on Petri dishes and placed in a laboratory dryer at 37ºC for 24 h.

Scaffold fabrication

The synthesis of the scaffolds began with the preparation of PLGA solution by dissolving 5.2 g of PLGA in 50 ml of DCM. Then the solution was placed on a magnetic stirrer (400 rpm) for 24 h. Meanwhile, 4.707 g of sodium chloride (NaCl, POCh, Gliwice, Poland) with sieved crystal diameters ranging from 400 to 600 μm were weighed on 10 dishes, into which 5 ml of the previously prepared PLGA solution was poured. The next step in preparing the scaffolds was to mix NaCl, which acted as a porogen, with the PLGA solution using a spatula until the solvent partially evaporated and has the form of a thick “paste”. The prepared paste was placed in syringes (5 ml volume), which hubs were cut off and covered with the parafilm. The syringes were left under the fume hood until the solvent evaporated completely. In the next stage, the obtained cylinders were cut into 2 mm thick slices.

In order to completely remove salt, the scaffolds were placed in a beaker with distilled water, which was changed every few hours until the water conductivity stabilized at a constant level on 1 μS/cm. The whole process took 4 days. After this time, the scaffolds were collected and left to dry on filter paper and then were placed on a Petri dish and left in a laboratory dryer at 37ºC until completely dried.

Microscopic observations

Both scaffolds and microsphere morphology were assessed with optical microscopes (Stereo Discovery V8 and Axiovert, both from Carl Zeiss, respectively). Samples were carefully placed on a mirror plate and then pictures were taken. The measurements were performed for 100 pores and 250 microspheres using the ImageJ software. In order to determine the porosity of scaffolds, the sum of the pore areas (measured in ImageJ program) was divided by the area of the photo, and the result was multiplied by 100.

***In vitro* studies**

Human mesenchymal stem cells (ATCC® CCL-1™, American Type Culture Collection, Manassas, VA, USA) were used for cell culture. Both microspheres and scaffolds were sterilized by immersion in ethyl alcohol for 24 h and then exposed to a UV lamp for 30 min. Scaffolds (1 per well) and microspheres (5 mg per well) were placed in a 24-well plate (Avantor, VWR). The culture was carried out at 37°C and at 5% CO_2. As a next step, the density of the cell suspension was determined so that each well contained the same number of hMSCs (20,000 cells per well). The basal medium (Mesenchymal Stem Cell Growth Medium 2, PromoCell GmbH, Heidelberg, Germany) was added to half of the wells, while to the other half was filled with differentiation medium. It consisted of a basal medium enriched with L-ascorbic acid (300 μM, 1%, Sigma-Aldrich, USA), dexamethasone (10 nM, 0.02%, Sigma-Aldrich, USA) and β-glycerophosphate disodium salt (10 mM, 1%, Sigma-Aldrich, USA).

Live/dead fluorescent staining was used to examine the viability and physiological activity of hMSC cells, by which the presence of live and dead cells could be determined. A solution consisting of phosphate buffer saline (PBS, VWR), propidium iodide (PI, Sigma-Aldrich, Germany), and calcein AM (Sigma-Aldrich, Germany) was used. Both substances were used in the following ratio 1 mg of PI and 1 mg of calcein per 1 ml of PBS. 300 μl of live/dead solution was poured into each well and then incubated for 10 min in a dark place. After 3, 7, and 14 days of cell culture establishment, microscopic observations were carried out using a fluorescence microscope AxioVert 40 (Carl Zeiss, Germany).

Additionally, phalloidin and DAPI staining was performed as to compare the cytoskeletal features of cells in basal and osteogenic medium. First, the medium was removed and the cells were rinsed with PBS enriched with magnesium and calcium ions (Sigma-Aldrich). Then a 3.7% formaldehyde solution (Sigma-Aldrich) was added to the cells for 20 min. As a next step, the cells were rinsed again with PBS solution. In the last step, 0.1% Triton X-100 solution was added to the wells and left there for 5 min. As time passed, the solution was removed and the cells were rinsed with distilled water. After the described procedure, staining dyes were added. First, phalloidin was added to the wells and left in the dark overnight. The following day, the cells were rinsed again with PBS, and DAPI was added. Further steps were the same as for phalloidin. Microscopic observations were carried out using a fluorescence microscope AxioVert 40 (Carl Zeiss, Germany).

LDH and ALP assays

To test lactate dehydrogenase (LDH) and alkaline phosphatase (ALP) activity 500 µl of 1% Triton X-100 solution (Sigma-Aldrich) was added into each culture well and then placed on a laboratory shaker (Grant-bio, Sunflower Mini-Shaker, PS-3D, 40 rpm) for 50 min. Meanwhile, a working solution was prepared by mixing 125 µl of solution A (INT/sodium lactate, Takara, Saint-Germain-en-Laye, France) and 5.625 ml of solution B (catalyst (A) diaphoresis/NAD, Takara, Saint-Germain-en-Laye, France). The solution of 0.5M HCl (POCh, Gliwice, Poland) acted as a stop solution.

After 50 min, 50 µl of the contents of each well were poured into a 24-well plate. In the next step, 50 µl of working solution was poured into each well and the samples prepared this way were put away for 8 min in the dark, necessary for the reaction to occur. After this time, 50 µl of stop solution was poured into the wells in order to stop the proceeding reaction. The final step to assess LDH activity was the measurement of absorbance for a wavelength of 492 nm (FluoStar Omega, BMG Labtech, Ortenberg, Germany).

For the ALP assay, exactly the same sample culture plates were used as for the LDH assay. While the plates were on the laboratory shaker for 50 min, a working solution was prepared by dissolving 1 tablet of p-nitrophenol in ALP buffer (0.1M diethanolamine, 0.1% Triton X-100, 1 mM MgCl · 6 H_2O, Sigma-Aldrich). 1M NaOH solution (POCh, Gliwice, Poland) acted as a stop solution. After 50 min, 25 µl of the contents of the wells were poured into a 24-well plate followed by 125 µl of working solution. To incubate the samples, they were left for 30 min at 37°C. After this time, 63 µl of stop solution was poured into each well. The final step of the assessment was to measure the absorbance for a wavelength of 405 nm (FluoStar Omega, BMG Labtech, Ortenberg, Germany). In order to learn precisely about the differentiation potential of cells, the outcome of ALP was divided by cell number so that the results present the activity of ALP osteogenic marker per one cell.

Statistics

Data are presented as an average ± standard deviation. Statistical analysis was obtained using a one-way analysis of variance (one-way ANOVA) followed by the post-hoc LSD Fisher test using OriginLab software. Probability values lower than 0.05: $p^* < 0.05$, $p^{**} < 0.01$, $p^{***} < 0.001$ were considered statistically significant.

Results and Discussions

Microscopic observations

The obtained PLGA microspheres are characterized by a relatively high regularity of shape and a smooth surface (FIG. 1A). In the images, the variation in terms of their size is visible. After analysis of the histogram, it can be seen that the size scatter is almost symmetrical (FIG. 1B). The most frequently occurring microspheres (29% of the total fraction) were in the range of diameters from 90 to 100 µm. Microspheres with diameters in the 80-90 µm and 100-110 µm ranges accounted for 18% of the total each. Microspheres with the smallest diameters (60-70 µm) were the least numerous, accounting for 5.5% of the total and those with the largest diameters, i.e., 120-130 µm (5% of the total) and 130-140 µm (5.5% of the total) ranges. Thus, it can be seen that the diameters of the largest microspheres were practically twice as large as those of the smallest ones. In summary, a large number of medium-sized microspheres in the 80-110 µm range was obtained. The median size of the microspheres was 95 µm.

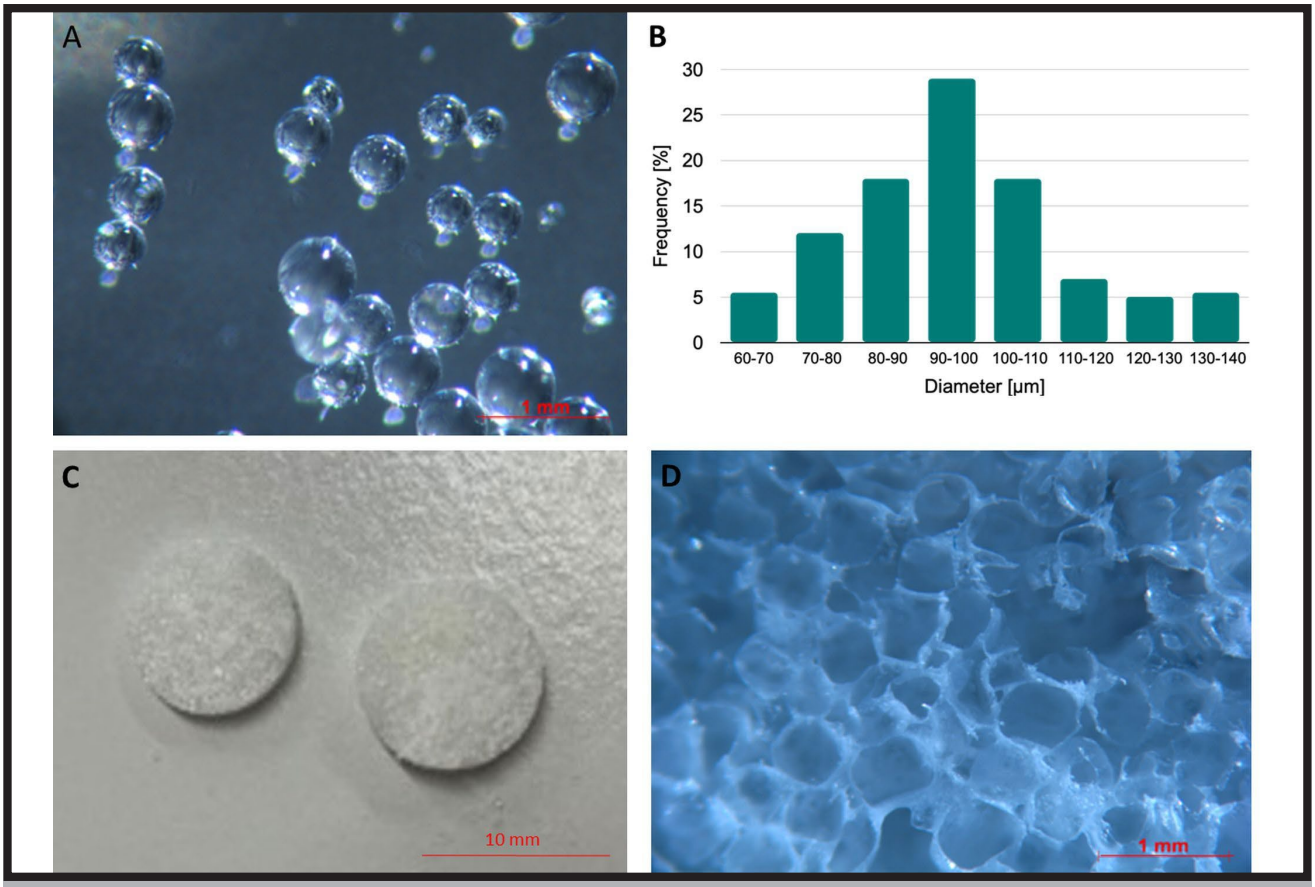

FIG. 1. Morphology (A) and size distribution (B) of PLGA microspheres. Gross morphology (C) and microstructure (D) of PLGA scaffolds. Scale bar (A, D) = 1 mm, (C) = 10 mm.

As shown in FIG. 1C the scaffolds had the form of cylinders 10 mm in diameter and 3 mm in height. Under higher magnification (FIG. 1D), one can observe that they consist of pores with size 360 μm ± 74 μm. The porosity of the scaffolds was 82.1% ± 4.2%. In the scaffolds we can see both concave and convex surfaces. It has been shown that topography and microstructure are very important cues regulating a variety of biological phenomena such as differentiation, morphogenesis, or cell migration [13]. Werner et al. noticed that concave surfaces promote efficient cell migration, whereas convex surfaces promote osteogenic differentiation as convexity leads to cell body flattening [14]. That morphology modification is accompanied by an increase in the level of laminine, which eventually leads to enhanced osteogenic differentiation [13].

***In vitro* studies**

To assess cell morphology phalloidin/DAPI staining and live/dead staining were performed. Already after 7 days significant differences concerning cells shape were noticeable. In differentiation medium cells were more spread and had characteristic polygonal shape, whereas cells cultured in basal medium were more elongated as shown by staining of the cytoskeletal actin fibers (by phalloidin) and nuclei (by DAPI) (FIG. 2A, FIG. 2B). It is also noticeable that the number of cells in basal medium is larger than in differentiation medium. After 14 days it is possible to distinguish certain changes in cell morphology after live/dead staining.

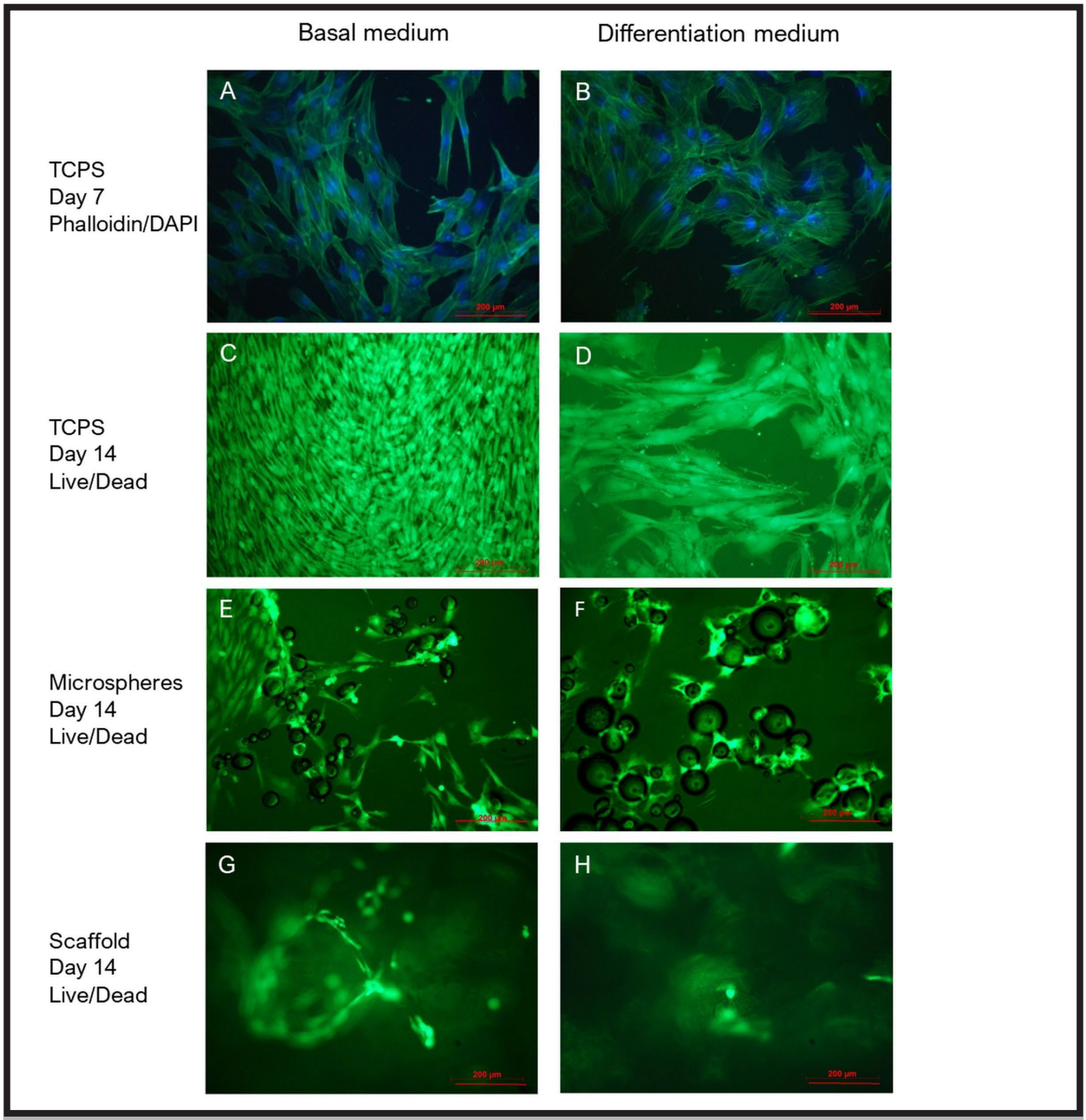

FIG. 2. Fluorescence microscopy images of hMSC cells on: TCPS on day 7 after seeding in basal medium (A) and differentiation medium (B) and on day 14 after seeding in basal medium (C) and differentiation medium (D); microspheres on 14 day after seeding in basal medium (D) and differentiation medium (E); scaffolds on day 14 after seeding in basal medium (G) and differentiation medium (H); phalloidin/DAPI staining (A, B) and live/dead staining (C-H); scale bar 200 μm.

Cells cultured on tissue culture polystyrene (TCPS) in basal medium occurred in larger numbers compared to those cultured in differentiation medium (FIG. 2C, FIG. 2D). The same tendency as regards proliferation was observed for cells cultured on microspheres and scaffolds (FIGs 2E-H). After 14 days of hMSCs culturing, the number of cells in basal medium was much higher than in differentiation medium. Additionally, cells in differentiation medium exhibited distinct morphological characteristics indicative of differentiation towards osteogenic lineage, but their proliferation was reduced. This observation indicates that supplements added to differentiation medium impacted cell behavior as proliferation was reduced due to enhanced osteogenic differentiation.

The results of ALP and LDH assessment confirmed observations described for microscopic studies. As shown by LDH assay (FIGs 3 A,C,E) for all the time points proliferation was more efficient for hMSCs cultured on TCPS, microspheres and scaffolds in basal medium than those cultured in differentiation medium. On day one, the number of cells was similar for all materials in both basal and differentiation media. For the next days, number of cells was gradually increasing. The most dynamic growth of cells was noticed from day 7 to 14 from cell seeding. Cells proliferated similarly on 3D constructs. However, proliferation was always more efficient for cell cultures in basal medium rather than differentiation medium. Similar results were obtained by Rumian et al., as the cells proliferated efficiently on PLGA scaffolds throughout the experiment [8].

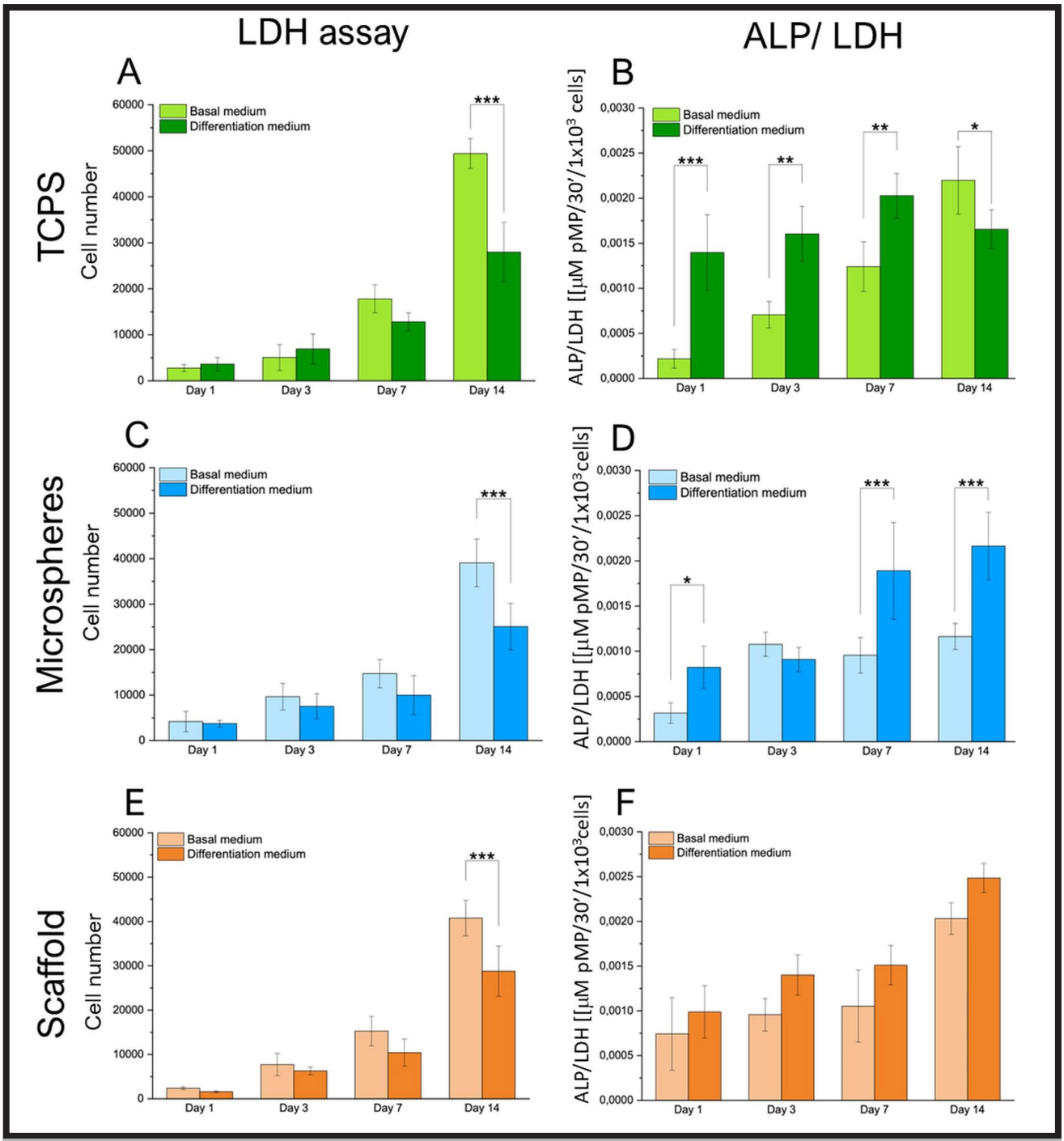

FIG. 3. LDH assay results for: A – microspheres, C – scaffolds, E – TCPS; ALP/LDH results for: B – microspheres, D – scaffolds, F – TCPS, $p^{*} < 0.05$, $p^{**} < 0.01$, $p^{***} < 0.001$ as compared cells cultured in different media. $p^{\#} < 0.05$, $p^{\#\#} < 0.01$ as compared to cells cultured on TCPS on respective time point.

The ALP activity related to cell number tested by LDH assay was used to evaluate the osteogenic differentiation potential of the hMSC as a function of culture time. In the case of cells seeded on TCPS (FIG. 3B), the ALP activity was rising vigorously in differentiation medium as compared to basal medium up to day 7. On day 14, ALP activity significantly dropped for cells cultured in differentiation medium. For cells cultured on the microspheres (FIG. 3D) amount of this marker was lower than on TCPS. On the scaffolds (FIG. 3F), the ALP activity was the same as on TCPS. This observation indicates that differentiation medium, as expected, promoted cell ALP activity. Nevertheless, for cells cultured on scaffolds on day 14, ALP activity in basal medium was the same as in differentiation medium. It is worth noticing that significant statistical differences between days 1 and 14 for each material were observed. This is a very promising result, suggesting that signals transduced by the microspheres and scaffolds can activate cells for osteogenic differentiation even without supplementing the medium with osteogenic factors. Similar results concerning cell number and ALP expression for hMSC were obtained by Rutledge et al. Both, cell number and activity of ALP increased slowly till day 7, then more dynamic growth was observed. However, the most efficient cell growth was observed for cells seeded on TCPS, whereas more efficient ALP expression was observed for cells seeded on PLGA scaffolds [15].

Conclusions

The PLGA microspheres obtained by emulsification method were non-porous and had a median size of 95 μm. The PLGA scaffolds obtained by the solvent casting/porogen leaching method had a microstructure with porosity of 82.1% ± 4.2% and a pore size of 360 μm ± 74 μm that mimics spongy bone. The LDH test proved that more cells on day 14 were present in cultures with basal medium rather than differentiation medium, but cell proliferation was the same on the scaffolds, microspheres and control TCPS. hMSC osteogenic differentiation potential, as expected, was enhanced in differentiation medium. However, for respective time points, cells exhibited higher ALP activity in basal medium when cultured on the scaffolds as on control TCPS. On day 14 cells cultured on the scaffolds in basal medium exhibited the same osteogenic potential as those cultured in differentiation medium. Thus, both microspheres and porous scaffolds were found more suitable for promotion of cell adhesion, proliferation, and differentiation, even when cultured in a medium not supplemented with osteogenic differentiation factors. In clinical conditions, when mechanical support is needed, we recommend implantation of the scaffolds. However, the application of microspheres can be considered when a low-invasive administration of the cell-biomaterial construct is required.

Acknowledgements

This study was supported from the subsidy (No 16.16.160.557) for the AGH University of Krakow.

ORCID iD

K. Walczak: https://orcid.org/0009-0000-5896-7132
M. Krok-Borkowicz: https://orcid.org/0000-0002-9415-0282
E. Pamuła: https://orcid.org/0000-0002-0464-6189

References

[1] Ansari M.: Bone tissue regeneration: biology, strategies and interface studies. Progress in Biomaterials 8 (2019) 223-237.
[2] Zhu G., Zhang T., Chen M., Yao K., Huang X., Zhang B., Li Y., Liu J., Wang Y., Zhao Z.: Bone physiological microenvironment and healing mechanism: Basis for future bone-tissue engineering scaffolds. Bioactive Materials 6 (2021) 4110-4140.
[3] Henkel J., Woodruff M., Epari D., Steck R., Glatt V., Dickinson I., Choong P., Schuetz M., Hutmacher D.: Bone regeneration based on tissue engineering conceptions - a 21st century perspective. Bone Research 3 (2013) 216-248.
[4] Asadi N., Del Bakhshayesh A., Davaran S., Akbarzadeh A.: Common biocompatible polymeric materials for tissue engineering and regenerative medicine. Materials Chemistry and Physics 242 (2020) 122528.
[5] Kumar P., Dehiya B., Sindhu A.: Bioceramics for hard tissue engineering applications. International Journal for Applied Engineering Research 13 (2018) 2744-2752.
[6] Turnbull G., Clarke J., Picard F., Riches P., Jia L., Han F., Li B., Shu W.: 3D bioactive composite scaffolds for bone tissue engineering. Bioactive Materials 3 (2018) 278-314.
[7] Chan B., Leong K.: Scaffolding in tissue engineering: general approaches and tissue-specific considerations. European Spine Journal 17 (2008) 467-479.
[8] Rumian Ł., Wojak I., Scharnweber D., Pamuła E.: Resorbable scaffolds modified with collagen type I or hydroxyapatite: in vitro studies on human mesenchymal stem cells. Acta of Bioengineering and Biomechanics 15 (2013) 61-67.
[9] Gupta V., Khan Y., Berkland C., Laurencin C., Detamore M.: Microsphere-based scaffolds in regenerative engineering. Annual Review of Biomedical Engineering 19 (2017) 135-161.
[10] Mielan B., Pamuła E.: Optimizing manufacturing conditions of polymer microspheres as cell carriers for modular tissue engineering. Engineering of Biomaterials 155 (2020) 2-9.
[11] Liu S., Cai M., Deng R., Wang J., Liang R., Zhu J.: fabrication of porous polymer microparticles with tunable pore size and density through the combination of phase separation and emulsion-solvent evaporation approach. Korea-Australia Rheology Journal 26 (2014) 63-71.
[12] Mielan B., Sousa D., Krok-Borkowicz M., Eloy P., Dupont C., Lamghari M., Pamuła E.: Polymeric microspheres/cells/extracellular matrix constructs produced by auto-assembly for bone modular tissue engineering. international Journal of Molecular Science 22 (2021) 7897.
[13] Rougerie P., Silva dos Santos R., Farina M., Anselme K.: Molecular mechanisms of topography sensing by osteoblasts: An update. Applied Sciences 11 (2021) 1791.
[14] Werner M., Blanquer S.B.G., Haimi S.P., Korus G., Dunlop J.W.C., Duda G.N., Grijpma D.W., Petersen A.: Surface curvature differentially regulates stem cell migration and differentiation via altered attachment morphology and nuclear deformation. Advanced Science News 4 (2017) 1600347.
[15] Rutledge K. E., Cheng Q., Jabbarzadeh E.: Modulation of inflammatory response and induction of bone formation based on combinatorial effects of resveratrol. Journal of Nanomedicine and Nanotechnology 7 (2016) 350.

OPTIMIZATION OF THE CALCIUM CARBONATE PARTICLES MANUFACTURING PROCESS BY THE PRECIPITATION METHOD AND BIOLOGICAL EVALUATION WITH MG-63 CELLS

Iwona Pudełko-Prażuch*, Karolina Wojtanek, Elżbieta Pamuła

AGH University of Krakow,
Faculty of Materials Science and Ceramics,
Department of Biomaterials and Composites,
al. A. Mickiewicza 30, 30-059 Krakow, Poland
*e-mail: ipudelko@agh.edu.pl

Abstract

As a natural mineral, calcium carbonate ($CaCO_3$) is widely investigated for various medical applications. It is a biocompatible material characterized by high degradation rate and great osteoconductivity. Many researchers evaluate $CaCO_3$ in the form of particles as a candidate for use in drug delivery systems. In this study we present an optimization of the process of producing $CaCO_3$ particles by the precipitation method with the use of combinations of different time of ultrasound treatment and surfactant concentrations used. Depending on the synthesis conditions, various sizes of particles were fabricated. The particles were loaded with sodium alendronate (Aln, 5% or 10% by weight) with a relatively high encapsulation efficiency between 40 and 50%, depending on the amount of Aln added and the drug loading of approximately 9% for both cases. MG-63 osteoblast-like cells were contacted with 10% wt./vol extracts of fabricated particles to assess their cytotoxicity. None of the extracts investigated was found to be cytotoxic. Furthermore, an in vitro study in direct contact of MG-63 cells with particles suspended in culture medium was performed. The results showed that the fabricated particles are cytocompatible with osteoblast-like MG-63 cells. However, the higher the concentration of the particle suspension and the greater the amount of alendronate present in the solution, the lower the metabolic activity of the cells was measured. The presented method of $CaCO_3$ particles manufacturing is simple, cost-effective, and allows one to fabricate particles of the required size and shape that are cytocompatible with MG-63 cells in defined concentrations of particle suspensions.

Keywords: *calcium carbonate microparticles, sodium alendronate, drug delivery system, MG-63 cells, bone tissue regeneration, particle size optimization*

[Engineering of Biomaterials 170 (2023) 20-27]

doi:10.34821/eng.biomat.170.2023.20-27

Submitted: 2023-09-08, Accepted: 2023-10-04, Published: 2023-10-06

Introduction

Calcium carbonate ($CaCO_3$) is a natural biological mineral that has gained considerable interest in numerous scientific and industrial areas [1-3]. Several factors make $CaCO_3$ popular and attractive: low price, wide availability, high surface area, and ease of synthesis [1-4]. Furthermore, calcium carbonate is characterized by good biocompatibility, biodegradability, osteoconductivity [1,3,5], pH sensitivity [2,3,6], and the ability to release drugs [1,2,6,7]; however, it is not regarded as osteoinductive [8]. Importantly, $CaCO_3$ is a material that has been approved by the US Food and Drug Administration (FDA) and the European Food Safety Agency (EFSA) as a food additive and nutrient source added to food [2,3]. $CaCO_3$ has been confirmed to have a faster resorption rate compared to hydroxyapatite [5] with comparable bone formation activity [6]. It may improve gene expression and exhibits a high degradation rate [4] and great osteoconductivity [6]. $CaCO_3$ nanoparticles have been reported to promote osteogenic differentiation of human bone marrow mesenchymal stem cells *in vitro* [4]. Due to its features, $CaCO_3$ in the form of particles appears to be an ideal candidate for use in drug delivery systems [1,7,9,10]. Manufacturing process of $CaCO_3$ is simple [10] and the drug release rate can be controlled by changing the size, shape, or composition of the particles [2,3]. The significant advantage of $CaCO_3$ particles is their degradability which eliminates the need to remove the delivery system after treatment [6]. $CaCO_3$ has been reported to be a carrier of different drugs and bioactive substances, such as doxorubicin [1], gentamicin [6], tetracycline hydrochloride [7] or doxorubicin hydrochloride [10].

Sodium alendronate (Aln) is a hydrophilic amphiprotic [11] and nitrogen-containing drug [12-14] that is approved by the FDA [15]. It belongs to the bisphosphonate class of drugs and is widely used for the treatment of bone diseases [11-14,16]. The action of Aln is to inhibit bone resorption by inducing osteoclast apoptosis, while improving osteoblast recruitment, differentiation, and bone remodelling activity [11,14,17,18]. Furthermore, it has been reported to increase bone mineral density [12,19] and improve the osteogenesis of bone marrow mesenchymal stem cell (BMSCs) and mesenchymal stromal cells (MSCs) [13,14]. Sodium alendronate has been widely investigated for local delivery. Different materials are being used to encapsulate Aln, such as polymers [19-22] and ceramics [23-26]. However, to the best of our knowledge, alendronate-loaded $CaCO_3$ particles require more in-depth studies. Thus, in this work, we aimed to manufacture calcium carbonate particles loaded with sodium alendronate for local drug delivery in bone tissue with the use of a simple, safe, low-cost, and effective precipitation method.

Materials and Methods

Materials

Sodium carbonate (Na_2CO_3), calcium chloride hexahydrate ($CaCl_2 \cdot 6H_20$), TWEEN 20, o-phtaldialdehyde (OPA), resazurin (Alamar Blue assay), calcein AM and propidium iodide were provided by Sigma Aldrich, Germany. Minimal essential medium (MEM), fetal bovine serum (FBS), penicillin/streptomycin (PS), amino acids and sodium pyruvate were purchased from PAN Biotech, Germany. Edetic acid (EDTA) was purchased from POCH, Poland, phosphate buffered saline (PBS) from VWR Life Science, and sodium alendronate (Aln) was provided by Polpharma S.A. Poland.

Manufacturing of calcium carbonate particles

To prepare $CaCO_3$ particles (CCPs), the precipitation method from aqueous solutions of Na_2CO_3 and $CaCl_2$ was used. In brief, the 0.33 M Na_2CO_3 solution was mixed with the 0.33 M $CaCl_2$ solution in a 1:1 ratio, while stirring at a speed of 2000 rpm [10,27]. The stirring was continued for 10 min, followed by centrifugation for 15 min at 5000 rpm (MPW-351R, MPW Med. instruments, Poland). Subsequently, the supernatant was discarded and 10 mL of ultra-high quality water (UHQ-water, produced in Direct-Q 3UV, Merck Millipore, USA) was added to the tube. The particles were resuspended and centrifuged again. The supernatant was removed, and the process was repeated three times. The particles were then frozen at -80ºC and freeze dried (Christ Alpha 1–2 LDplus, Martin Christ, Germany).

Effect of ultrasounds on the size of particles

The effect of ultrasounds on the size of the particles was checked by introducing ultrasound treatment into the manufacturing process. Basically, Na_2CO_3 and $CaCl_2$ were mixed in the presence of an ultrasonic probe for 5, 10 and 15 min (Vibra Cell VCX130, Sonics, USA), followed by stirring with the magnetic stirrer for 10 min at 2000 rpm. The subsequent stages were carried out without any changes.

Effect of surfactant on the size of particles

To evaluate the influence of the presence of surfactant on the particles size, TWEEN 20 was added to the solutions of Na_2CO_3 and $CaCl_2$ at different concentrations – 0.5, 1 and 2%. Basic solutions containing different amounts of TWEEN 20 were mixed and the process was carried out as previously described.

Effect of ultrasound combined with surfactant on the size of particles

The combination of both previously mentioned factors was assessed as well. To do so, Na_2CO_3 and $CaCl_2$ solutions with different concentrations of TWEEN 20 (0.5, 1 and 2%) were mixed in the presence of an ultrasonic probe for different times (5, 10 and 15 min), followed by stirring. As previously, the next stages of the manufacturing process were carried out without any changes.

Encapsulation of sodium alendronate

Sodium alendronate was encapsulated in CCPs during the manufacturing process (Aln-CCPs). In brief, a different amount of the drug (5 and 10% relative to the theoretical mass of the particles) was dissolved in the Na_2CO_3 solution and mixed with $CaCl_2$ under adequate conditions.

Characterization of particles

The particles were observed with the use of a scanning electron microscope (SEM Apreo 2, Thermo Scientific, USA). The size was checked with dynamic light scattering (DLS), expressed as mean and standard deviation (SD), and confirmed with SEM observations. Encapsulation efficiency (EE) and drug loading (DL) were examined with the use of an OPA assay. To do so, the alendronate loaded particles were dissolved in EDTA, adjusted to a pH value equal to 8 with 1 M NaOH, at a concentration of 1 mg/mL. Then, 50 µL of the solution was transferred to a black 96-well plate, 50 µL of OPA reagent was added and fluorescence was measured (λ_{ex} = 340 nm, λ_{em} = 460 nm, FLUOstar Omega, BMG Labtech, Germany).

Biological evaluation with extracts

The extracts of empty and loaded particles were tested with osteoblast-like MG-63 cells. To obtain 10% extracts, the particles (after being exposed for 20 min to UV irradiation) were immersed in MEM supplemented with 10% FBS, 1% penicillin/streptomycin, 0.1% amino acids, and 0.1% sodium pyruvate for 24 h. In an adequate number of wells, 10,000 cells suspended in 100 µL of MEM per well were seeded. Culture was carried out for 24 h at 37°C in a 5% CO_2 atmosphere. After that time, the medium was exchanged into extracts (filtered with a 0.2 µm filter) and the cells were cultured in them for another 24 h. The Alamar Blue assay and live/dead staining were then performed to verify the metabolic activity and morphology of the cells, respectively. For Alamar Blue, 150 µL of a 10% resazurin solution in a medium was added to each well and incubated for 3 h. Then 100 µL of the solution was transferred from each well to a black 96-well plate and the fluorescence was measured (λ_{ex} = 544 and λ_{em} = 590 nm). To calculate the level of resazurin reduction, we used the following formula (1):

$$\%\ \text{resazurin reduction} \frac{S_x - S_{blank}}{S_{reduced} - S_{blank}} \cdot 100\% \qquad (1)$$

where:
S_x – fluorescence of the samples,
S_{blank} – 0% reduction of resazurin,
$S_{reduced}$ – 100% reduction of resazurin.

To conduct live/dead staining, calcein AM (0.1%) and propidium iodide (0.1%) were dissolved in phosphate buffered saline solution (PBS). We added 100 µL of the solution to each well and incubated it for 20 min in darkness. The cells were then observed with a fluorescent microscope (ZEISS Axiovert 40 CFL) with a ZEISS HXP 120 C metal halide illuminator.

Cytocompatibility test

To evaluate cytocompatibility, MG-63 cells were evaluated in direct contact with the particles. Briefly, suspensions of different concentrations of empty and loaded particles were prepared. The particles were sterilized by exposing them twice to UV irradiation. In an adequate number of wells, 10,000 cells suspended in 100 µL of MEM per well were seeded. Culture was carried out for 24 h at 37°C in a 5% CO_2 atmosphere. Later, the medium was exchanged into particle suspensions and the culture was continued for another 24 h. After that time, the Alamar Blue assay and live/dead staining were performed, as described in 'Biological evaluation with extracts' section.

Statistical analysis

The results are presented as mean ± standard error of the mean (S.E.M.). The analysis of the results obtained was conducted using a one-way analysis of variance (one-way ANOVA) followed by the post-hoc LSD Fisher test in OriginLab software. Probability values less than 0.05: $p^*<0.05$, $p^{**}<0.01$, $p^{***}<0.001$ were considered statistically significant.

Results and Discussions

$CaCO_3$ particles were fabricated using the precipitation method. Different times of ultrasound treatment and different concentrations of TWEEN 20 were used to determine the best conditions for obtaining particles. The results show that both factors have a significant influence on the size of the particles (FIG. 1).

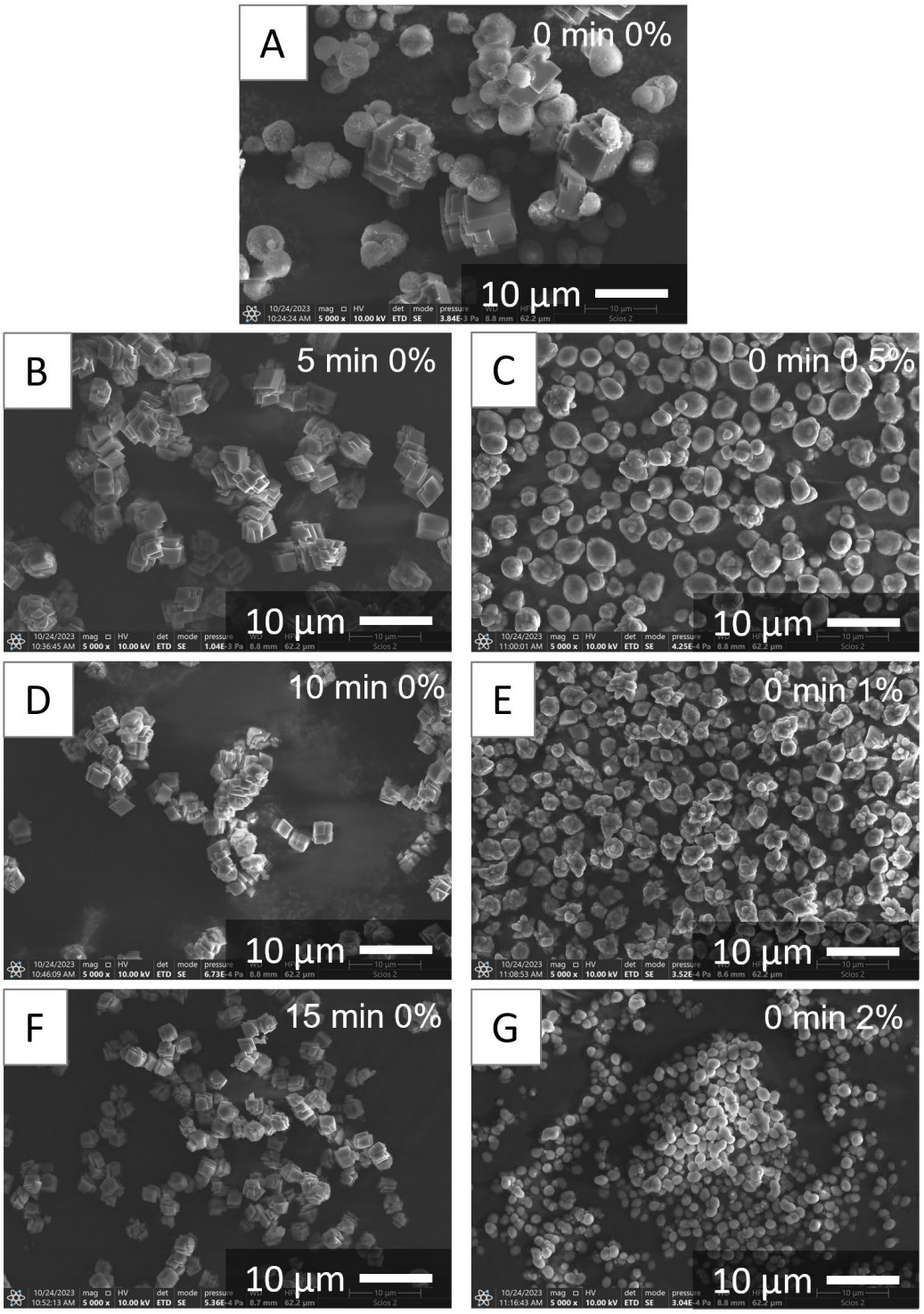

FIG. 1. Effect of ultrasound treatment time (0, 5, 10 and 15 min) and TWEEN 20 concentration (0%, 0.5%, 1%, 2%) on the size and microstructure of $CaCO_3$ particles obtained during the precipitation process.

The use of ultrasound makes it possible to obtain smaller particles, while the presence of a surfactant stabilizes the system, so that the formed particles have a round shape. The longer the ultrasound treatment time used, the smaller the particles. Moreover, the addition of surfactant appears to allow smaller particle sizes to be obtained; however, too high concentration may lead to the agglomeration of $CaCO_3$ particles (FIGs 2 G-I). Furthermore, the presence of the surfactant makes it possible to fabricate particles of round shape. $CaCO_3$ particles manufactured without TWEEN 20 are visible to have a cubic shape, indicating that the transformation of vaterite into calcite has occurred [28]. This means that the surfactant works as a stabilizer of a vaterite phase of $CaCO_3$ crystals. Interestingly, when no ultrasound treatment is performed, the particles obtained with all concentrations of TWEEN 20 belong to the same population; however, the more surfactant used, the more agglomerated particles are. Furthermore, there is no statistically significant difference between particles manufactured without the addition of surfactant at various times of ultrasound treatment. That indicates that 5 min is enough for the precipitation reaction to occur and a longer time does not affect the size.

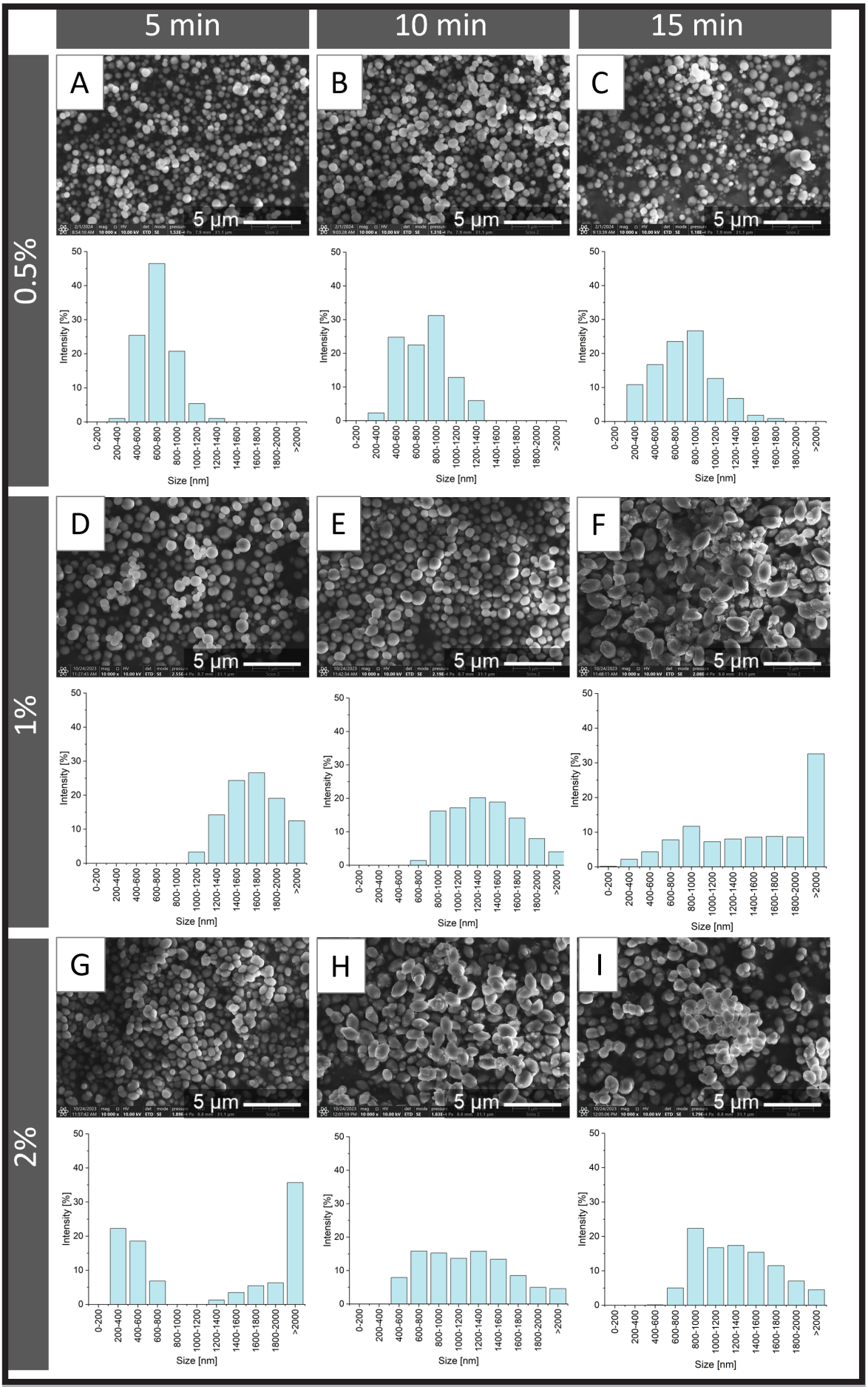

FIG. 2. SEM microphotographs and size distribution of different types of $CaCO_3$ particles submitted to different combinations of ultrasound treatment time and surfactant concentration.

The combination of ultrasound treatment and the addition of TWEEN 20 allows to obtain particles of different sizes (TABLE 1), depending on the conditions. According to the literature, various sizes of $CaCO_3$ particles may be obtained with the use of different methods of manufacturing and the conditions used. The size of $CaCO_3$ particles has been reported to vary between 50 nm and 6 μm while the precipitation method is used with most particles greater than 1 μm [29]. However, the use of different additives during the precipitation allows to control the size of the obtained particles. This corresponds to the findings of other scientists that presented particles of different sizes [4,6,7,10,29]. The smallest particles in our investigation were manufactured when 5 min of ultrasound and 0.5% of surfactant were used and have a size of 0.7 ± 0.2 μm. On the other hand, the size distribution in the case of this sample is relatively wide. Therefore, the most optimal conditions appear to be 10 min of ultrasound with the addition of 1% TWEEN 20. The size is slightly higher, but the size distribution is narrower. Smaller particles may be obtained with the use of different combinations; however, apart from the size distribution, the shape of the particles changes. Furthermore, the use of different methods of manufacturing can be utilized to fabricate much smaller particles [4,6]. We chose 10 min of ultrasound treatment and the addition of 1% TWEEN 20 as the most optimal conditions and they were used for further investigation. The addition of Aln has no impact on the shape of the obtained particles. Furthermore, the size of the Aln-loaded particles, fabricated under the same conditions, is not significantly different compared to the empty particles (TABLE 2). Although the precipitation method is simple and relatively effective, it is nonetheless a manual process. Its automation would improve the accuracy of the technique and allow obtaining particles of a specific, predefined size. Future research should focus on the use of other surfactants, as well as the use of homogenizers and/or a milling process to obtain smaller particles.

The encapsulation efficiency decreased, while the drug loading increased with the amount of alendronate used. Different polymers have been reported to encapsulate sodium alendronate, and the efficiency was dependent on the material used. Jing *et al*. presented three compositions of alendronate-loaded nanoparticles based on poly(lactic-co-glycolic acid) (PLGA) in which both encapsulation efficiency and drug loading exceeded 70% [20]. Moreover, chitosan nanoparticles have been reported to have EE in the range of 40 to 70% [22]. On the other hand, Miladi *et al*. demonstrated polycaprolactone (PCL) particles that were characterized by EE and DL in the ranges of 15-34% and 2-21%, respectively [21]. According to the literature, calcium carbonate particles are being used to encapsulate various drugs. The encapsulation efficiency of gentamicin in $CaCO_3$ particles was reported to be 38% with a drug loading of 25% [6]. Sudareva *et al*. showed $CaCO_3$ particles loaded with doxorubicin with a drug content greater than 90% [30]. Encapsulation efficiency and drug loading are highly dependent on the drug and material used. However, in this study, EE was relatively high in each case and varied between 40 and 50%, depending on the addition of Aln and DL was approximately 9% for the addition of 5 and 10% of alendronate (TABLE 2).

TABLE 1. Size of $CaCO_3$ particles fabricated under different conditions.

Time of ultrasound treatment [min]	Surfactant concentration [%]	Size ± SD [μm]
0	0	17.8 ± 7.5
0	0.5	2.5 ± 0.7
0	1	2.2 ± 0.2
0	2	1.8 ± 0.1
5	0	5.1 ± 1.7
5	0.5	0.7 ± 0.2
5	1	2.1 ± 0.5
5	2	1.4 ± 0.4
10	0	4.6 ± 2.1
10	0.5	0.8 ± 0.2
10	1	1.3 ± 0.1
10	2	1.1 ± 0.4
15	0	4.4. ± 1.1
15	0.5	0.8 ± 0.3
15	1	1.3 ± 0.1
15	2	1.2 ± 0.1

Osteoblast-like MG-63 cells were cultured in 10% extracts of manufactured particles to evaluate their potential cytotoxicity. Cells were contacted with extracts for 24 h and then their metabolic activity was checked (FIG. 3 A) and live/dead staining was performed (FIG. 3 B). Compared to the control, cells activity was significantly lower while cultured in extracts of each type of particles. Interestingly, the resazurin reduction in the case of samples containing Aln was higher than that of empty $CaCO_3$ particles. No decrease of greater than 70% compared to the control can be observed, which means no toxicity of the investigated extracts according to ISO 10993-5 [31]. Interestingly, the metabolic activity of cells cultured in the extracts of Aln-loaded particles (both 5 and 10%) was higher compared to empty ones. This suggests that sodium alendronate supports the proliferation of osteoblast-like cells.

To evaluate the cellular response of $CaCO_3$ particles, osteoblast-like MG-63 cells were cultured in direct contact with particle suspensions. Depending on the type of particles, the metabolic activity of cells (FIGs 4 A,C,E) was decreasing with increasing concentration of particles present in MEM. However, for empty particles, the relevant decrease is observed for the concentration of 100 mg/mL. In the case of 10% addition of alendronate, concentrations of 50 and 100 mg/mL were toxic for cells; however, a statistically significant decrease, compared to the control (0 mg/mL), can also be observed for lower concentrations (FIGs 4 A,C,E). It is visible that cell activity is significantly lower for a concentration of 100 mg/mL, even for empty particles.

TABLE 2. Characteristics of $CaCO_3$ particles loaded with alendronate.

Time of ultrasound treatment [min]	Surfactant concentration [%]	Addition of alendronate [%]	Size ± SD [μm]	Encapsulation efficiency (EE) [%]	Drug loading (DL) [%]
10	1	0	1.3 ± 0.1	-	-
10	1	5	1.1 ± 0.2	49.6 ± 2.0	9.2 ± 0.4
10	1	10	1.1 ± 0.3	39.7 ± 1.3	9.6 ± 0.3

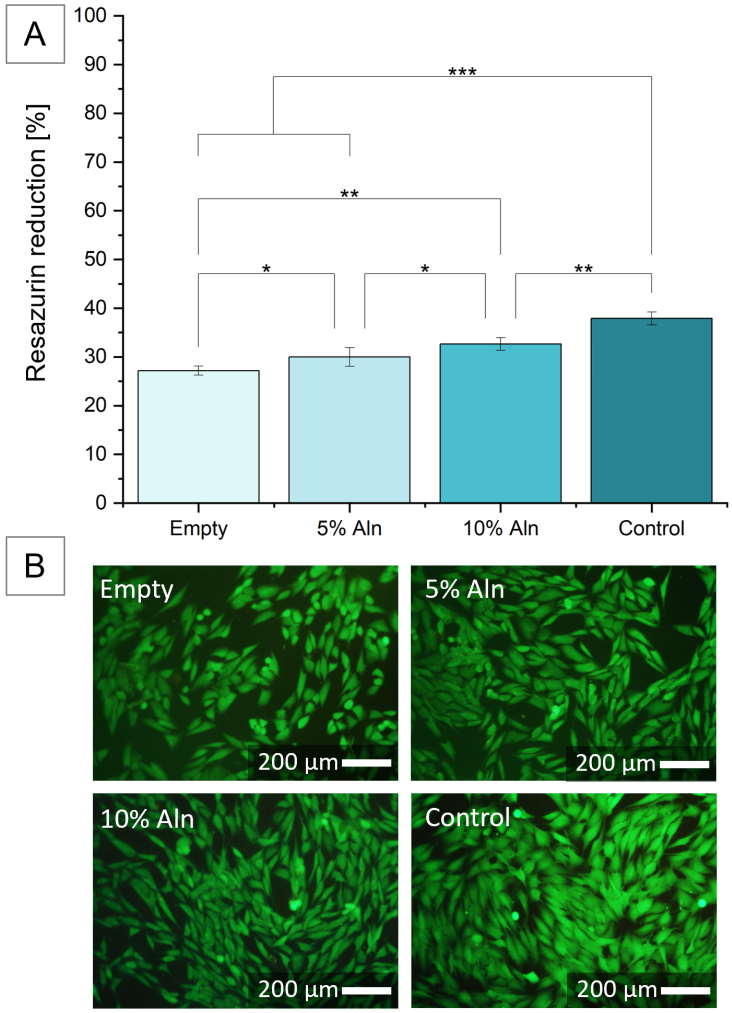

FIG. 3. Metabolic activity (A) and live/dead staining (B) of MG-63 cells cultured in the presence of 10% extracts of empty particles, particles loaded with 5% and 10% addition of sodium alendronate and in MEM, as control. No decrease in metabolic activity greater than 70% compared to the control can be observed.

However, the metabolic activity of cells when contacted with empty particles is not significant for lower concentrations, which is comparable to the results of other researchers [32,33]. The resazurin reduction is lower, compared to the control for each suspension of particles containing Aln, indicating that alendronate may be toxic for MG-63 cells, especially at higher doses. Although the $CaCO_3$ particles with Aln showed great performance during the study with extracts, it is not the case when we study them in direct contact with the particle suspensions.

Conclusions

The aim of this research was to optimize the process of manufacturing calcium carbonate particles with sodium alendronate encapsulated and to investigate their cytotoxicity and cytocompatibility with osteoblast-like MG-63 cells. Different times of ultrasound treatment and concentrations of surfactant were used to control the size of the fabricated particles. The use of 0.5% of surfactant combined with 5 min of ultrasounds allows to obtain the smallest particles. However, a combination of 1% and 10 min gives slightly larger particles, but with a narrower size distribution. The extracts of empty and loaded particles (5 or 10% alendronate) were tested with MG-63 cells and did not show signs of cytotoxicity. Furthermore, the cellular response of the particles was investigated by contacting MG-63 cells with particles suspended in a culture medium. According to the results, a higher concentration of sodium alendronate present in the system may be toxic to the investigated cells. However, the particles are cytocompatible with MG-63 cells in lower concentrations even with a 10% addition of sodium alendronate. Depending on the application and requirements, different compositions may be used to obtain particles of the required size. The presented process is simple, low-cost, and effective to fabricate calcium carbonate particles that are cytocompatible with MG-63 cells.

Acknowledgements

This research was funded by the Program "Excellence Initiative – Research University" and the subsidy (No 16.16.160.557) for the AGH University of Krakow. The authors would like to acknowledge the access to the Laboratory of Electron Microscopy of the Faculty of Materials Science and Ceramics at the AGH University of Krakow.

ORCID iD

I. Pudełko-Prażuch: https://orcid.org/0000-0002-1024-9374
K. Wojtanek: https://orcid.org/0009-0008-8975-930X
E. Pamuła: https://orcid.org/0000-0002-0464-6189

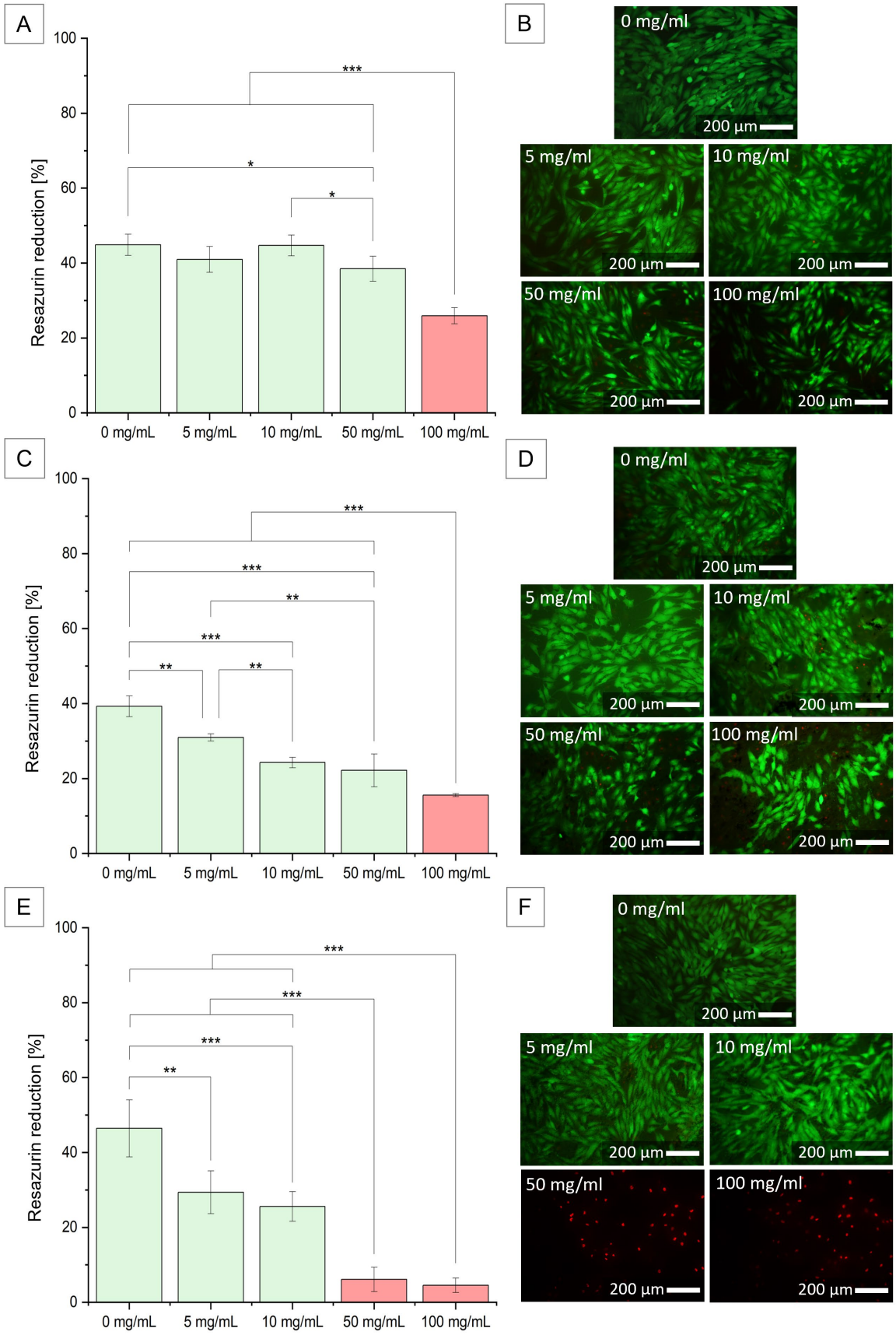

FIG. 4. Metabolic activity (A, C, E) and live/dead staining (B, D, F) of MG-63 cells cultured in direct contact with empty particles (A, B), particles loaded with 5% (C, D) and 10% (E, F) addition of sodium alendronate. A high concentration (100 mg/mL) of particles is toxic for MG-63 cells in each case. A lower resazurin reduction is observed for particles loaded with sodium alendronate compared to empty ones, which indicates the toxicity of sodium alendronate in high doses.

References

[1] Li L., Yang Y., Lv Y., Yin P., Lei T.: Porous calcite $CaCO_3$ microspheres: Preparation, characterization and release behavior as doxorubicin carrier. Colloids and Surfaces B: Biointerfaces 186 (2020) 110720.

[2] Tan C., Dima C., Huang M., Assadpour E., Wang J., Sun B., Kharazmi M., Jafari S. M.: Advanced $CaCO_3$-derived delivery systems for bioactive compounds. Advances in Colloid and Interface Science 309 (2022) 102791.

[3] Ferreira A.M., Vikulina A.S., Volodkin D.: $CaCO_3$ crystals as versatile carriers for controlled delivery of antimicrobials. Journal of Controlled Release 328 (2020) 470-489.

[4] Li X., Yang X., Liu X., He W., Huang Q., Li S., Feng Q.: Calcium carbonate nanoparticles promote osteogenesis compared to adipogenesis in human bone-marrow mesenchymal stem cells. Progress in Natural Science: Materials International 28(5) (2018) 598-608.

[5] Bang L.T., Son N.A., Long B.D., Nhung N.T.H.: Calcium carbonate coating on Ti-6Al-4 V by carbonate diffusion in calcium source at room temperature. Materials Today: Proceedings 66 (2022) 2929-2932.

[6] Memar M.Y., Adibkia K., Farajnia S., Kafil H.S., Maleki Dizaj S., Ghotaslou R.: Biocompatibility, cytotoxicity and antimicrobial effects of gentamicin-loaded $CaCO_3$ as a drug delivery to osteomyelitis. Journal of Drug Delivery Science and Technology 54 (2019) 101307.

[7] Ren B., Chen X., Du S., Ma Y., Chen H., Yuan G., Li J., Xiong D., Tan H., Ling Z., Chen Y., Hu X., Niu X.: Injectable polysaccharide hydrogel embedded with hydroxyapatite and calcium carbonate for drug delivery and bone tissue engineering. International Journal of Biological Macromolecules 118 (2018) 1257-1266.

[8] Sirkiä S.V., Qudsia S., Siekkinen M., Hoepfl W., Budde T., Smått J.-H., Peltonen J., Hupa L., Heino T.J., Vallittu P.K.: Physicochemical and biological characterization of functionalized calcium carbonate. Materialia 28 (2023) 101742.

[9] Yang T., Ao Y., Feng J., Wang C., Zhang J.: Biomineralization inspired synthesis of $CaCO_3$-based DDS for pH-responsive release of anticancer drug. Materials Today Communications 27 (2021) 102256.

[10] Wei Y., Sun R., Su H., Xu H., Zhang L., Huang D., Liang Z., Hu Y., Zhao L., Lian X.: Synthesis and characterization of porous $CaCO_3$ microspheres templated by yeast cells and the application as pH value-sensitive anticancer drug carrier. Colloids and Surfaces B: Biointerfaces 199 (2021) 111545.

[11] Ezzati Nazhad Dolatabadi J., Hamishehkar H., Eskandani M., Valizadeh H.: Formulation, characterization and cytotoxicity studies of alendronate sodium-loaded solid lipid nanoparticles. Colloids and Surfaces B: Biointerfaces 117 (2014) 21-28.

[12] Dong J., Tao L., Abourehab M.A.S., Hussain Z.: Design and development of novel hyaluronate-modified nanoparticles for combo-delivery of curcumin and alendronate: fabrication, characterization, and cellular and molecular evidences of enhanced bone regeneration. International Journal of Biological Macromolecules 116 (2018) 1268-1281.

[13] Lee J.Y., Kim S.E., Yun Y.-P., Choi S.-W., Jeon D.I., Kim H.-J., Park K., Song H.-R.: Osteogenesis and new bone formation of alendronate-immobilized porous PLGA microspheres in a rat calvarial defect model. Journal of Industrial and Engineering Chemistry 52 (2017) 277-286.

[14] Wei P., Yuan Z., Jing W., Huang Y., Cai Q., Guan B., Liu Z., Zhang X., Mao J., Chen D., Yang X.: Strengthening the potential of biomineralized microspheres in enhancing osteogenesis via incorporating alendronate. Chemical Engineering Journal 368 (2019) 577-588.

[15] Öz U.C., Toptaş M., Küçüktürkmen B., Devrim B., Saka O.M., Deveci M.S., Bilgili H., Ünsal E., Bozkır A.: Guided bone regeneration by the development of alendronate sodium loaded in-situ gel and membrane formulations. European Journal of Pharmaceutical Sciences 155 (2020) 105561.

[16] Zhao Q., Cheng D.-Q., Tao M., Ning W.-J., Yang Y.-J., Meng K.-Y., Mei Y., Feng Y.-Q.: Rapid magnetic solid-phase extraction based on alendronate sodium grafted mesoporous magnetic nanoparticle for the determination of trans-resveratrol in peanut oils. Food Chemistry 279 (2019) 187-193.

[17] Hur W., Park M., Lee J.Y., Kim M.H., Lee S.H., Park C.G., Kim S.N., Min H.S., Min H.J., Chai J.H., Lee S.J., Kim S., Choi T.H., Choy Y.B.: Bioabsorbable bone plates enabled with local, sustained delivery of alendronate for bone regeneration. Journal of Controlled Release 222 (2015) 97-106.

[18] Kellesarian S.V., Abduljabbar T., Vohra F., Malignaggi V.R., Malmstrom H., Romanos G.E., Javed F.: Role of local alendronate delivery on the osseointegration of implants: a systematic review and meta-analysis. International Journal of Oral and Maxillofacial Surgery 46(7) (2017) 912-921.

[19] De Molon R.S., Fiori L.C., Verzola M.H., Belluci M.M., De Souza Faloni A.P., Pereira R.M.R., Tetradis S., Orrico S.R.: Long-term evaluation of alendronate treatment on the healing of calvaria bone defects in rats. Biochemical, histological and immunohistochemical analyses. Archives of Oral Biology 117 (2020) 104779.

[20] Jing C., Chen S., Bhatia S.S., Li B., Liang H., Liu C., Liang Z., Liu J., Li H., Liu Z., Tan H., Zhao L.: Bone-targeted polymeric nanoparticles as alendronate carriers for potential osteoporosis treatment. Polymer Testing 110 (2022) 107584.

[21] Miladi K., Sfar S., Fessi H., Elaissari A.: Encapsulation of alendronate sodium by nanoprecipitation and double emulsion: From preparation to in vitro studies. Industrial Crops and Products 72 (2015) 24-33.

[22] Miladi K., Sfar S., Fessi H., Elaissari A.: Enhancement of alendronate encapsulation in chitosan nanoparticles. Journal of Drug Delivery Science and Technology 30 (2015) 391-396.

[23] Zhao Q., Xiao D., Li Y., Chen X., Hu K., Luo X., Yang F., Yang Z., Liu J., Feng G., Liu J., Feng D., Duan K.: Repair of rabbit femoral head necrosis by release of alendronate and growth differentiation factor-5 from injectable alginate/calcium phosphate carriers. Materials Today Communications 33 (2022) 104530.

[24] Aryan N., Behpour M., Benvidi A., Jookar Kashi F., Azimzadeh M., Zare H.R.: Evaluation of sodium alendronate drug released from TiO_2 nanoparticle doped with hydroxyapatite and silver-strontium for enhancing antibacterial effect and osteoinductivity. Materials Chemistry and Physics 295 (2023) 126934.

[25] Zhao X., Zhu L., Fan C.: Sequential alendronate delivery by hydroxyapatite-coated maghemite for enhanced bone fracture healing. Journal of Drug Delivery Science and Technology 66 (2021) 102761.

[26] Lee J.H., Ko I.H., Jeon S.-H., Chae J.-H., Chang J.H.: Microstructured hydroxyapatite microspheres for local delivery of alendronate and BMP-2 carriers. Materials Letters 105 (2013) 136-139.

[27] Ali Said F., Bousserrhine N., Alphonse V., Michely L., Belbekhouche S.: Antibiotic loading and development of antibacterial capsules by using porous $CaCO_3$ microparticles as starting material. International Journal of Pharmaceutics 579 (2020) 119175.

[28] Trushina D.B., Bukreeva T.V., Kovalchuk M.V., Antipina M.N.: $CaCO_3$ vaterite microparticles for biomedical and personal care applications. Materials Science and Engineering: C 45 (2014) 644-658.

[29] Salomão R., Costa L.M.M., Olyveira G.M.D.: Precipitated Calcium Carbonate Nano-Microparticles: Applications in Drug Delivery. Advances in Tissue Engineering & Regenerative Medicine: Open Access 3(2) (2017) 336-340.

[30] Sudareva N., Suvorova O., Saprykina N., Vlasova H., Vilesov A.: Doxorubicin delivery systems based on doped $CaCO_3$ cores and polyanion drug conjugates. Journal of Microencapsulation 38 (2021) 164-176.

[31] International Organization for Standarization: ISO 10993-5:2009, Biological evaluation of medical devices - Part 5: Tests for in vitro cytotoxicity.

[32] Zhong Q., Li W., Su X., Li G., Zhou Y., Kundu S.C., Yao J., Cai Y.: Degradation pattern of porous $CaCO_3$ and hydroxyapatite microspheres in vitro and in vivo for potential application in bone tissue engineering. Colloids Surf. B Biointerfaces 143 (2016) 56-63.

[33] Pietryga K., Panaite A.-A., Pamuła E.: Composite scaffolds enriched with calcium carbonate microparticles loaded with epigallocatechin gallate for bone tissue regeneration. Engineering of Biomaterials 166 (2022) 12-21.